Exit time distribution in spherically symmetric two-dimensional domains

J.-F. Rupprecht,[1] O. Bénichou,[1] D. S. Grebenkov,[2] and R. Voituriez[3,1]

[1]*Sorbonne Universités, UPMC Univ Paris 06, UMR 7600, Laboratoire de Physique Théorique de la Matière Condensée, 4 Place Jussieu, 75005, Paris, France.*
[2]*Laboratoire de Physique de la Matière Condensée (UMR 7643), CNRS – Ecole Polytechnique, F-91128 Palaiseau Cedex France*
[3]*Sorbonne Universités, UPMC Univ Paris 06, UMR 8237, Laboratoire Jean Perrin, 4 Place Jussieu, 75005, Paris, France.*

(Dated: September 29, 2014)

The distribution of exit times is computed for a Brownian particle in spherically symmetric two-dimensional domains (disks, angular sectors, annuli) and in rectangles that contain an exit on their boundary. The governing partial differential equation of Helmholtz type with mixed Dirichlet-Neumann boundary conditions is solved analytically. We propose both an exact solution relying on a matrix inversion, and an approximate explicit solution. The approximate solution is shown to be exact for an exit of vanishing size and to be accurate even for large exits. For angular sectors, we also derive exact explicit formulas for the moments of the exit time. For annuli and rectangles, the approximate expression of the mean exit time is shown to be very accurate even for large exits. The analysis is also extended to biased diffusion. Since the Helmholtz equation with mixed boundary conditions is encountered in microfluidics, heat propagation, quantum billiards, and acoustics, the developed method can find numerous applications beyond exit processes.

arXiv:1409.7624v1 [physics.comp-ph] 26 Sep 2014

I. INTRODUCTION

First passage time (FPT) processes are ubiquitous in physics, chemistry, and biology, with numerous examples of applications ranging from enzymes searching for specific DNA sequences to animal foraging [1–4]. The problem of finding the FPT distribution has direct implications in the fields of neutron or light scattering [5] and in biological modelling. For instance, the time needed for an ion to find an open channel is a limiting step in the kinetics of the neurological process of phototransduction [6]. The role of the confining domain on the FPT distribution of a regulation protein to a specific DNA site can account for the bursting dynamics in gene regulation [7].

When a target is located on the boundary of a confining domain, the FPT can be understood as the first exit time from the domain through an opening (e.g., a "hole") on the boundary. Hitherto most studies have focused on the mean first passage time (MFPT) of a Brownian particle to a small exit, which is called the narrow escape problem [8–11]. For a starting position which is far enough from the boundary, the FPT distribution was shown to be dominated by its exponential tail in the limit of a large confining volume: hence the MFPT was sufficient to characterize the whole FPT distribution, except for the very short–times region [3, 12, 13]. Note that the short-time behavior of this distribution was approximately accounted for by a Dirac distribution whose contribution vanished in the small exit limit. A generic multi-exponential representation of the FPT distribution in domains with heterogeneous distribution of targets was proposed in [14]. Some progress to precisely describe the short-time behavior of the FPT distribution has been recently achieved. For instance, Isaacson and Newby proposed a uniform asymptotic approximation of the FPT distribution in the small exit limit for 3D confining domains [11].

In the present article we address the following question: what is the distribution of the first passage time to an arbitrarily large exit? To answer this question, we consider a particle diffusing in a confined spherically symmetric two-dimensional domain $\Omega \subset \mathbb{R}^2$ which is periodic along the angular coordinate θ and bounded in the radial coordinate r. Examples of such domains are disks, angular sectors, and annuli. The analysis is also applicable to rectangles. The boundary of Ω is reflecting except for an absorbing patch on the surface through which the particle can escape. In spherically symmetric 2D domains, a Fourier expansion of the survival probability along the periodic coordinate θ can be performed. We adapt the resolution schemes described in [15] to solve the Helmholtz equation with mixed boundary conditions satisfied by the survival probability. Our approach leads to both exact and approximate expressions for the FPT distribution and for the moments of the exit time (Sec. II B). As a result, we managed to describe the whole distribution of first passage times and their moments for the escape problem with arbitrary exit size. The approximate solution, which is shown to be exact in the limit of

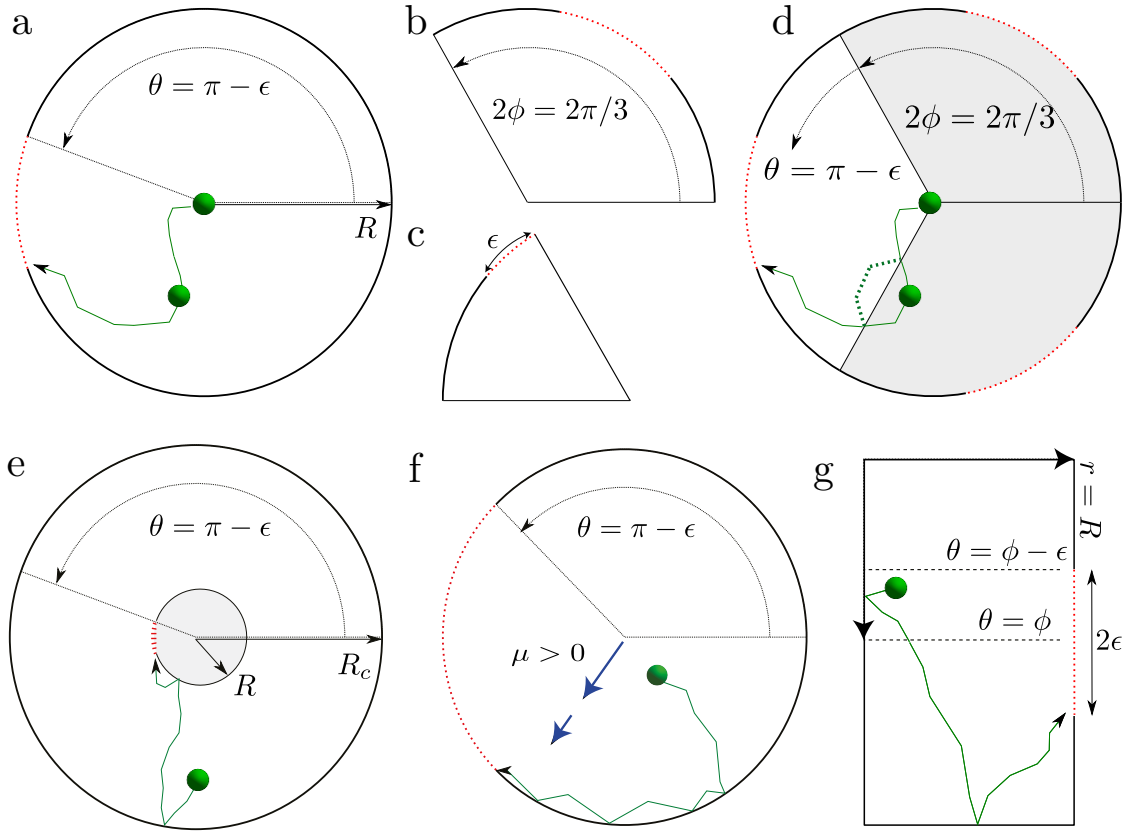

FIG. 1: (Color Online) A Brownian particle (green circle) diffuses in a domain Ω whose boundary is reflecting (solid line) except for an absorbing exit (dashed red line). **(a)** Ω is a disk of radius R and the exit arclength is $2R\epsilon$; **(b)** Ω is an angular sector of half-aperture $\phi = \pi/3$, with reflecting rays at $\theta = 0$ and $\theta = 2\phi$; **(c)** Ω is an angular sector of total aperture $\phi = \pi/3$, with reflecting rays at $\theta = 0$ and $\theta = \phi$ (the exit arclength is $R\epsilon$); **(d)** Ω is a disk with 3 regularly spaced exits of arclength $2R\epsilon$ on the boundary. The distribution of exit times through any of the three regularly spaced exits (case **d**) is identical to the distribution of exit times through a single centered exit within an angular sector of half-aperture $\phi = \pi/3$ (case **b**). We sketch the reflection principle by representing the trajectory of the particle inside the disk with three exits by solid green line, while its image trajectory inside one of the angular sector of half-aperture $\phi = \pi/3$ is shown by dashed green line; **(e)** Ω is an annulus of radii R and R_c with an exit of half-width ϵ located on the inner radius R; **(f)** Ω is a disk and the Brownian particle is advected by a radial flow field $\vec{v}(r) = \mu D\, \vec{r}/r^2$, with $\mu > 0$, corresponding to an outward drift (blue arrows); **(e)** Ω is a rectangle of total width R and height 2ϕ.

a target of vanishing width, is in fact accurate over the whole range of times scales even for large exit sizes.

We apply this approach to the following domains: disks, angular sectors, annuli and rectangles (see Fig. 1). Table I summarizes the new results in this paper. For Brownian particles confined in an angular sector, we provide the exact explicit expression for the MFPT and for the variance of the exit time (Sec. II D 2). In the case of a disk, we obtain an expression for the Fourier coefficients of the MFPT which is much simpler than the earlier expression from Ref. [8]. We point out that the variance of the exit time for an arbitrary starting point was previously known only through its leading order term in the small exit limit [12]. We also compute the exact skewness and excess kurtosis of the exit time for a Brownian particle started from an arbitrary point within an angular sector. Away from a boundary layer near the exit, we show that the ratio of the standard deviation to the MFPT is close to 1, the skewness to 2, and the excess kurtosis to 6, indicating that the FPT distribution can be well approximated by an exponential distribution, in contrast to the statement of Ref. [19].

We exhibit the following non-intuitive result on the MFPT of Brownian particles confined to an annulus of radii R and R_c (Sec. III A): under an analytically determined criteria, the MFPT is an optimizable function of the radius R_c. This result is based on an approximate expression for the MFPT which is in quantitative agreement with numerical simulations even for a large exit size and for arbitrary

TABLE I: Summary of the results presented in this paper and comparison to previous publications. T is the mean first passage time (MFPT) to an exit of width ϵ from an arbitrary starting position $\vec{r}_0$. The considered geometries are described in Fig. 1.

	Previous results		This paper	
	Moments	FPT distribution	Moments	FPT distribution
Disk	T: exact explicit [8, 16]	$\epsilon \ll 1$, $\vec{r}_0$ away	Exact explicit	Exact (non-explicit)
	Averaged variance [16]	from boundaries [12]	T, variance	Approximate (explicit)
			skewness, kurtosis	
Angular Sector		$\epsilon \ll 1$, $\vec{r}_0$ away	Exact explicit	Exact (non-explicit)
		from boundaries [12]	T, variance	Approximate (explicit)
			skewness, kurtosis	
Annulus	T: $(\epsilon, R/R_c) \ll 1$ [17]	$\epsilon \ll 1$, $\vec{r}_0$ away	Approximate T	Exact (non-explicit)
		from boundaries [12]	for all R_c	Approximate (explicit)
Rectangle	T: $(\epsilon, \phi/R) \ll 1$ [17]	$\epsilon \ll 1$, $\vec{r}_0$ away	Approximate T	Exact (non-explicit)
	Exact non-explicit [6]	from boundaries [12]	for all R	Approximate (explicit)
Drift	T: $\epsilon \ll 1$ [18]		Approximate T	Exact (non-explicit)
$\vec{v}(r) = \frac{\mu D}{r^2}\,\vec{r}$	towards the exit		for all μ	Approximate (explicit)

radius R_c. In contrast to the classical narrow-escape formulas for the MFPT in 2D domains of Ref. [20] which are not valid for degenerate domains (in which one of dimensions is much smaller than the others), our approximate expression of the MFPT is accurate even in the extreme case $R_c = R$ which corresponds to a circle. Our approximate expressions are also accurate for rectangular confinements (Sec. III C).

In Sec. III B, we consider Brownian particles biased by a $1/r$ radial drift and confined in a disk. This situation is encountered in the biological modelling literature: the trajectories of marked proteins or tracers within the cytoplasm can be quantitatively described by an advection drift which models the effect of the intermittent active transport due to molecular motors stochastically binding and unbinding to microtubules [21].

In Sec. III D and Sec. III E, we explain why the FPT problem can be equivalently formulated in at least two other physical contexts. The first is a heat transfer problem [22, 23] in which the temperature in a room with adiabatic walls and an open window can be deduced from our solution for the FPT distribution to the window (Sec. III D). The second is a hydrodynamic problem in which the flow rate in a microchannel with ultra-hydrophobic walls [24–26] can be deduced from our explicit expressions for the MFPT to the exit (Sec. III E).

II. GENERAL FORMALISM AND APPLICATION TO ANGULAR SECTORS

A. Model and basic equations

We consider a Brownian particle confined in a bounded domain $\Omega \subset \mathbb{R}^2$, with an exit $\Gamma \subset \partial\Omega$ located on an otherwise reflecting boundary $\partial\Omega\backslash\Gamma$. The probabilistic description of this restricted diffusion relies on the diffusive propagator $\tilde{G}^{(t)}(\vec{r};\vec{r}_a)$, i.e., the probability density for a particle to move from an initial position $\vec{r} = (r,\theta)$ to a vicinity of the arrival position $\vec{r}_a$ in time t, without exiting the domain.

The diffusive propagator satisfies a backward diffusion equation [1, 27]

$$\frac{\partial \tilde{G}^{(t)}(\vec{r};\vec{r}_a)}{\partial t} = D\Delta \tilde{G}^{(t)}(\vec{r};\vec{r}_a), \tag{1}$$

where D is the diffusion coefficient, and Δ the Laplace operator acting on the initial position $\vec{r}$. The initial condition at $t=0$ on $\tilde{G}^{(t)}(\vec{r};\vec{r}_a)$ is given by a Dirac distribution $\delta(\vec{r}-\vec{r}_a)$,

$$\tilde{G}^{(t=0)}(\vec{r};\vec{r}_a) = \delta(\vec{r}-\vec{r}_a), \tag{2}$$

fixes the arrival position at $\vec{r}_a$, while the mixed boundary conditions incorporate the reflecting boundary with an absorbing exit:

$$\tilde{G}^{(t)}(\vec{r};\vec{r}_a) = 0, \qquad \vec{r}\in\Gamma, \tag{3}$$

$$\partial_n \tilde{G}^{(t)}(\vec{r};\vec{r}_a) = 0, \qquad \vec{r}\in\partial\Omega\backslash\Gamma, \tag{4}$$

where $\partial_n = \partial/\partial n$ is a shortcut notation for the normal derivative. The Dirichlet boundary condition (3) mimics the absorbing character of the exit Γ (i.e., the process is stopped once the particle hits the exit), while the Neumann boundary condition (4) means no flux across the remaining reflecting boundary $\partial\Omega\backslash\Gamma$. The mixed character of the boundary conditions presents the major challenge in solving this classical boundary value problem.

In this paper, we consider planar domains $\Omega = \{(r,\theta)\in\mathbb{R}^2 \ : \ R_c < r < R,\ 0<\theta<2\phi\}$ which in polar coordinates (r,θ) are 2ϕ-periodic along the angular coordinate θ and bounded in the radial coordinate r by R_c and R (e.g., disk ($\phi=\pi$) and angular sector shown in Fig. 1 for $R_c=0$). The exit Γ is an arc $\theta\in[\phi-\epsilon,\phi+\epsilon]$ within an otherwise reflecting boundary $\partial\Omega\backslash\Gamma$ at $r=R$. The boundary condition $r=R_c$ is reflecting. Note that the exit can also be located on the inner circle, in which case one writes $R<r<R_c$ instead of $R_c<r<R$. The angular sector geometry also accounts for the case of multiple regularly spaced exits within a disk. As illustrated on Fig. 1(c) for the case $n=3$, the exit through any of n regularly spaced exits of width 2ϵ within a disk can be equivalently represented as the exit through (i) a single opening of width 2ϵ at the center of an angular sector of width $2\pi/n$, or (ii) through a single opening of width ϵ in the corner of an angular sector of width π/n.

The time needed for the particle started at $\vec{r}_0=(r,\theta)$ to reach the exit is denoted as a random variable τ. The survival probability up to time t, denoted by $\tilde{S}^{(t)}(r,\theta)$, is the probability that the exit time τ is larger than t: $\tilde{S}^{(t)}(r,\theta) = \mathbb{P}\{\tau\geq t|\ X(0)=(r,\theta)\}$. Since the arrival position does not matter for the survival probability, $\tilde{S}^{(t)}(r,\theta)$ is simply obtained by integrating the diffusive propagator over the arrival positions $\vec{r}_a$:

$$\tilde{S}^{(t)}(r,\theta) = \int_\Omega \tilde{G}^{(t)}(r,\theta;\vec{r}_a)\ \mathrm{d}\vec{r}_a. \tag{5}$$

According to Eqs. (1 – 4), the survival probability satisfies the following equations [1, 27]

$$\frac{\partial \tilde{S}^{(t)}(r,\theta)}{\partial t} = D\Delta\tilde{S}^{(t)}(r,\theta), \qquad (r,\theta)\in\Omega \tag{6a}$$

$$\tilde{S}^{(t=0)}(r,\theta) = 1, \qquad (r,\theta)\in\Omega \tag{6b}$$

$$\tilde{S}^{(t)}(r,\theta) = 0, \qquad r=R,\quad \theta\in[\phi-\epsilon,\phi+\epsilon], \tag{6c}$$

$$\partial_r\tilde{S}^{(t)}(r,\theta) = 0, \qquad r=R,\quad \theta\in[0,\phi-\epsilon)\cup(\phi+\epsilon,2\phi], \tag{6d}$$

$$\partial_r S^{(t)}(r,\theta) = 0 \qquad r=R_c,\quad \theta\in[0,2\phi). \tag{6e}$$

$$\partial_\theta\tilde{S}^{(t)}(r,\theta) = 0 \qquad r\in[R_c,1],\quad \theta\in\{0,2\phi\}. \tag{6f}$$

where $\partial_r = \partial/\partial r$ is a shortcut notation for the radial derivative (note that here $\partial_r = \partial_n$), and the Laplace operator Δ in the polar coordinates is

$$\Delta = \frac{\partial^2}{\partial r^2} + \frac{1}{r}\frac{\partial}{\partial r} + \frac{1}{r^2}\frac{\partial^2}{\partial\theta^2}. \tag{7}$$

The last Eq. (6f) incorporates the reflecting boundary condition at the rays $\theta=0$ and $\theta=2\phi$ or, equivalently, the 2ϕ-periodicity of the domain.

In this article, we study the exit time statistics through the Laplace transform of the survival probability $\tilde{S}^{(t)}(r,\theta)$, defined for all $p \geq 0$ as

$$S^{(p)}(r,\theta) \equiv \int_0^\infty \exp(-p\,t)\,\tilde{S}^{(t)}(r,\theta)\mathrm{d}t. \tag{8}$$

The FPT probability density is $\tilde{\rho}^{(t)}(r,\theta) = -\frac{\partial \tilde{S}^{(t)}(r,\theta)}{\partial t}$. Alternatively, one can compute $\tilde{\rho}^{(t)}(r,\theta)$ through the inverse Laplace transform of

$$\rho^{(p)}(r,\theta) \equiv 1 - p\ S^{(p)}(r,\theta). \tag{9}$$

The series expansion of $\exp(-pt)$ in Eq. (8) yields

$$S^{(p)}(r,\theta) = \sum_{n=1}^{\infty} \frac{(-p)^{n-1}}{n!} \mathbb{E}\left[\tau_{(r,\theta)}^n\right], \tag{10}$$

from which the n-th moment of the exit time is

$$\mathbb{E}\left[\tau_{(r,\theta)}^n\right] = (-1)^{n-1}\ \left[\frac{\partial^{n-1} S^{(p)}(r,\theta)}{\partial p^{n-1}}\right]_{p=0}, \qquad n \geq 1. \tag{11}$$

In particular, the mean FPT (MFPT) to reach the exit from a starting point $\vec{r} = (r,\theta)$ reads

$$\mathbb{E}\left[\tau_{(r,\theta)}\right] \equiv \int_0^\infty t\,\tilde{\rho}^{(t)}(r,\theta)\,\mathrm{d}t = \int_0^\infty \tilde{S}^{(t)}(r,\theta)\,\mathrm{d}t = S^{(0)}(r,\theta). \tag{12}$$

Last, it is useful to introduce the global MFPT (GMFPT), denoted $\overline{\mathbb{E}\left[\tau\right]}$, as the MFPT averaged over all starting positions $\vec{r} = (r,\theta) \in \Omega$:

$$\overline{\mathbb{E}\left[\tau\right]} \equiv \frac{1}{|\Omega|} \int_\Omega \mathrm{d}\vec{r}\ \mathbb{E}\left[\tau_{\vec{r}}\right], \tag{13}$$

where $\mathrm{d}\vec{r}$ is the uniform measure over Ω.

We now consider the Laplace transform of Eq. (6a – 6f), which yields

$$D\ \Delta\ S^{(p)}(r,\theta) = p\ S^{(p)}(r,\theta) - 1, \qquad (r,\theta) \in \Omega, \tag{14a}$$

$$S^{(p)}(r,\theta) = 0, \qquad r = R, \quad \theta \in [\phi - \epsilon, \phi + \epsilon], \tag{14b}$$

$$\partial_r S^{(p)}(r,\theta) = 0, \qquad r = R, \quad \theta \in [0, \phi - \epsilon) \cup (\phi + \epsilon, 2\phi]. \tag{14c}$$

$$\partial_r S^{(p)}(r,\theta) = 0 \qquad r = R_c, \quad \theta \in [0, 2\phi), \tag{14d}$$

$$\partial_\theta S^{(p)}(r,\theta) = 0 \qquad r \in [R_c, R], \quad \theta \in \{0, 2\phi\}\,. \tag{14e}$$

The Laplace transform simplifies the resolution of a heat equation (6a) into the resolution of an inhomogeneous Helmholtz equation (14a). Solutions of the Helmholtz equation in cylindrical coordinates generally involve the modified Bessel functions of the first kind $I_n(r)$, defined as the solutions $y(x)$ of the differential equation

$$r^2 \frac{\partial^2 y}{\partial r^2} + r \frac{\partial y}{\partial r} - (r^2 + n^2) y = 0, \tag{15}$$

which are finite at $r = 0$ for positive n.

In the rest of this section we introduce dimensionless quantities $r \leftarrow r/R$, $S^{(p)} \leftarrow DS^{(p)}/R^2$, and $p \leftarrow R^2 p/D$, and define the following auxiliary function:

$$u^{(p)}(r,\theta) \equiv S^{(p)}(r,\theta) - S_\pi^{(p)}(r), \tag{16}$$

where $S_\pi^{(p)}(r)$ is the rotation invariant solution of Eq. (14a) satisfying $S_\pi^{(p)}(1) = 0$ and $\partial_r S_\pi^{(p)}(r) = 0$ at $r = R_c$. In the case of diffusion inside an angular sector (with $R_c = 0$), $S_\pi^{(p)}(r)$ can be written in terms of the zeroth-order modified Bessel function $I_0(z)$ of the first kind as

$$S_\pi^{(p)}(r) = \frac{1}{p}\left(1 - \frac{I_0(\sqrt{p}r)}{I_0(\sqrt{p})}\right) \tag{17}$$

(expression for the case $R_c > 0$ is provided in Table II). Note that if the entire boundary at $r = 1$ is absorbing (i.e., $\epsilon = \phi$), the solution of Eq. (14a) is $S^{(p)}(r,\theta) = S_\pi^{(p)}(r)$ [29].

In terms of the auxiliary function $u^{(p)}(r,\theta)$, Eqs. (14a – 14e) become

$$\Delta u^{(p)}(r,\theta) = p\, u^{(p)}(r,\theta), \qquad (r,\theta) \in \Omega \tag{18a}$$

$$u^{(p)}(r,\theta) = 0, \qquad r = 1, \qquad \theta \in [\phi-\epsilon, \phi+\epsilon], \tag{18b}$$

$$\partial_r u^{(p)}(r,\theta) = -\partial_r S_\pi^{(p)}(r), \qquad r = 1, \qquad \theta \in [0, \phi-\epsilon) \cup (\phi+\epsilon, 2\phi], \tag{18c}$$

$$\partial_r u^{(p)}(r,\theta) = 0 \qquad r = R_c, \qquad \theta \in [0, 2\phi). \tag{18d}$$

$$\partial_\theta u^{(p)}(r,\theta) = 0 \qquad r \in [R_c, 1], \qquad \theta \in \{0, 2\phi\}, \tag{18e}$$

Using the separation of variables method, we express a general solution of Eq. (18a) which satisfies the periodicity $\theta \to \theta + 2\phi$ as

$$u^{(p)}(r,\theta) = \frac{a_0^{(p)}}{2} f_0^{(p)}(r) + \sum_{n=1}^{\infty} a_n^{(p)} f_n^{(p)}(r) \cos\left(\frac{n\pi\theta}{\phi}\right), \qquad (r,\theta) \in [0,\ 1) \times [0, \phi]. \tag{19}$$

where the functions $f_n^{(p)}$ depend on the considered geometry. Since the unknown Fourier coefficients $a_n^{(p)}$ stand in front of $f_n^{(p)}$, one can choose an appropriate normalization of the functions $f_n^{(p)}$. We choose the normalization condition $f_n^{(p)}(1) = \phi/\pi$ $(n \geq 0)$. In the case of Brownian particles inside an angular sector ($R_c = 0$), $f_n^{(p)}$ are expressed in terms of modified Bessel functions $I_n(z)$ of the first kind:

$$f_n^{(p)}(r) = \frac{\phi}{\pi} \frac{I_{n\pi/\phi}(\sqrt{p}r)}{I_{n\pi/\phi}(\sqrt{p})}, \qquad n \geq 0. \tag{20}$$

The function $S_\pi^{(p)}(r)$ defined in Eq. (16) is

$$S_\pi^{(p)}(r) = \frac{1 - \frac{\pi}{\phi} f_0^{(p)}(r)}{p}. \tag{21}$$

The Fourier coefficients $a_n^{(p)}$ will be uniquely determined through the boundary conditions (18b) and (18c). Substituting Eq. (19) into Eqs. (18b) and (18c) leads to the system of equations

$$\frac{a_0^{(p)}}{2} + \sum_{n=1}^{\infty} a_n^{(p)} \cos\left(\frac{n\pi\theta}{\phi}\right) = 0, \qquad \theta \in [\phi-\epsilon, \phi], \tag{22a}$$

$$\left[\partial_r f_0^{(p)}\right]_{|r=1} \frac{a_0^{(p)}}{2} + \sum_{n=1}^{\infty} a_n^{(p)} \left[\partial_r f_n^{(p)}\right]_{|r=1} \cos\left(\frac{n\pi\theta}{\phi}\right) = -\left[\partial_r S_\pi^{(p)}\right]_{|r=1}, \qquad \theta \in [0, \phi-\epsilon), \tag{22b}$$

where the angular coordinate θ was limited to the half-range $[0, \phi]$ (instead of $[0, 2\phi]$) due to the symmetry of these equations with respect to the change $\theta \to 2\phi - \theta$ (this symmetry is also related to the reflection symmetry of the domain with respect to the ray $\theta = \phi$).

In the next section, we propose two schemes (exact and approximate) to solve Eqs. (22a) and (22b).

B. Resolution schemes

1. *Exact explicit expression for the MFPT in angular sector*

Let us first simplify previously known results in the case of the MFPT in a disk ($\phi = \pi$) and extend these results to angular sectors. Using the $p \ll 1$ asymptotic expansion,

$$\frac{I_n(\sqrt{p}r)}{I_n(\sqrt{p})} = r^n \left\{1 + \frac{\left(r^2-1\right) p}{4(1+n)}\right\} + \mathcal{O}(p^2), \qquad n \geq 0, \tag{23}$$

we show that in the particular case of the MFPT ($p = 0$), Eqs. (22a) and (22b) read

$$\frac{a_0^{(0)}}{2} + \sum_{n=1}^{\infty} a_n^{(0)} \cos(n\theta) = 0, \qquad \theta \in [\pi - \epsilon, \pi], \tag{24a}$$

$$\sum_{n=1}^{\infty} n a_n^{(0)} \cos(n\theta) = \frac{1}{2}, \qquad \theta \in [0, \pi - \epsilon). \tag{24b}$$

In Ref. [8], the solution of these equations was provided in the form:

$$a_0^{(0)} = \frac{\sqrt{2}}{\pi} \int_0^{\pi-\epsilon} \mathrm{d}x \frac{x \sin(x/2)}{\sqrt{\cos x + \cos\epsilon}}, \tag{25a}$$

$$a_n^{(0)} = \frac{1}{\sqrt{2}\pi} \int_0^{\pi-\epsilon} \mathrm{d}t \left(\frac{\partial}{\partial t} \int_0^t \mathrm{d}x \frac{x \sin(x/2)}{\sqrt{\cos x - \cos t}} \right) \left[P_n(\cos t) + P_{n-1}(\cos t) \right], \quad n \geq 1, \tag{25b}$$

where $P_n(x)$ are Legendre polynomials.

In fact, we show in Appendix A that these equations can be simplified as::

$$a_0^{(0)} = -2 \ln \left[\sin\left(\frac{\epsilon}{2}\right) \right], \tag{26a}$$

$$a_n^{(0)} = \frac{(-1)^{n-1}}{2n} \left[P_n(\cos\epsilon) + P_{n-1}(\cos\epsilon) \right], \qquad n \geq 1. \tag{26b}$$

We also extend these results to an angular sector of half-aperture ϕ and radius $r = 1$: $\Omega = \{(r, \theta) \in \mathbb{R}^2 \ : \ 0 \leq r < 1, \ 0 < \theta < 2\phi\}$. Under the change of variables $\hat{\theta} = \theta\pi/\phi$ and $\hat{\epsilon} = \epsilon\pi/\phi$, Eqs. (22a) and (22b) are reduced to Eqs. (24a), (24b) in the limit $p = 0$, from which

$$a_0^{(0)} = \alpha_0 \equiv -2 \ln \left[\sin\left(\frac{\epsilon\pi}{2\phi}\right) \right], \tag{27a}$$

$$a_n^{(0)} = \alpha_n \equiv \frac{(-1)^{n-1}}{2n} \left[P_n\left(\cos\frac{\epsilon\pi}{\phi}\right) + P_{n-1}\left(\cos\frac{\epsilon\pi}{\phi}\right) \right], \qquad n \geq 1. \tag{27b}$$

We conclude that the MFPT from the angular sector for a particle started at position (r, θ) is

$$\mathbb{E}\left[\tau_{(r,\theta)}\right] = \frac{1 - r^2}{4} + \frac{\alpha_0}{2}\frac{\phi}{\pi} + \frac{\phi}{\pi} \sum_{n=1}^{\infty} \alpha_n \ r^{n\pi/\phi} \ \cos\left(\frac{n\pi\theta}{\phi}\right), \tag{28}$$

where ϕ is the half-aperture of the angular sector, and ϵ is the half-width of the centered exit (see Fig. 1(b)). The GMFPT defined in Eq. (13) reads

$$\overline{\mathbb{E}\left[\tau\right]} \equiv \frac{2}{\phi} \int_0^{\phi} \int_0^1 r \, \mathrm{d}r \, \mathrm{d}\theta \ \mathbb{E}\left[\tau_{(r,\theta)}^n\right] = \frac{1}{8} + \frac{\alpha_0}{2}\frac{\phi}{\pi}. \tag{29}$$

To our knowledge, the results in Eqs. (27a), (27b), (28) and (29) are new.

Last, as described in Fig. 1(d), we recall that the exit through a window of width ϵ at the corner of the sector of angle π/m can be equivalently represented as the exit through any of m regularly spaced openings of width 2ϵ within a disk. In the limit of an infinite number of exits $m \to \infty$, ($\phi = \pi/m \to 0$) at a fixed ratio ϵ/ϕ, the MFPT of Eq. (28) tends to the MFPT to the fully absorbing boundary at $r = 1$, as expected [14, 30].

2. Exact resolution scheme for the survival probability

Now we solve the system of equations on the Fourier coefficients $a_n^{(p)}$ for an arbitrary value of p. We first introduce

$$\gamma_n^{(p)} \equiv 1 - \frac{\left[\partial_r f_n^{(p)}\right]_{r=1}}{n}, \qquad n \geq 1, \tag{30}$$

which we use to define the following function

$$F^{(p)}(\hat{\theta}) \equiv -\left[\partial_r S_\pi^{(p)}\right]_{|r=1} - \left[\partial_r f_0^{(p)}\right]_{|r=1} \frac{a_0^{(p)}}{2} + \sum_{n=1}^{\infty} a_n^{(p)} \gamma_n^{(p)} n \cos(n\hat{\theta}), \qquad \theta \in [0, \pi - \hat{\epsilon}). \tag{31}$$

For diffusion inside an angular sector, the explicit expression for $\gamma_n^{(p)}$ is

$$\gamma_n^{(p)} \equiv 1 - \frac{\sqrt{p}}{2n} \frac{\phi}{\pi} \frac{I_{n\pi/\phi-1}(\sqrt{p}) + I_{n\pi/\phi+1}(\sqrt{p})}{I_{n\pi/\phi}(\sqrt{p})}, \qquad n \geq 1, \tag{32}$$

where we have used the definition (20).

Under the change of variables $\hat{\theta} = \theta\pi/\phi$ and $\hat{\epsilon} \equiv \epsilon\pi/\phi$, Eqs. (22a) and (22b) read

$$\frac{a_0^{(p)}}{2} + \sum_{n=1}^{\infty} a_n^{(p)} \cos(n\hat{\theta}) = 0, \qquad \hat{\theta} \in [\pi - \hat{\epsilon}, \pi], \tag{33a}$$

$$\sum_{n=1}^{\infty} n a_n^{(p)} \cos(n\hat{\theta}) = F^{(p)}(\hat{\theta}), \qquad \hat{\theta} \in [0, \pi - \hat{\epsilon}), \tag{33b}$$

The problem of determining the Fourier coefficients $a_n^{(p)}$ from Eqs. (33a) and (33b) is closely related to the problem considered in Ref. [15] for a given function $F^{(p)}(\hat{\theta})$ which was independent of $a_n^{(p)}$. The crucial difference between the present case and the case considered in Ref. [15] is that the function $F^{(p)}(\hat{\theta})$ defined in Eq. (31) depends on the unknown Fourier coefficients $a_n^{(p)}$. In the rest of this section, we adapt the method of Ref. [15] to reduce Eqs. (33a) and (33b) to a linear system of equations for the Fourier coefficients.

We first assume that for $\hat{\theta} \in [0, \pi - \hat{\epsilon})$ we can define a function $h_1^{(p)}(t)$ such that

$$\frac{a_0^{(p)}}{2} + \sum_{n=1}^{\infty} a_n^{(p)} \cos(n\hat{\theta}) = \cos(\hat{\theta}/2) \int_{\hat{\theta}}^{\pi-\hat{\epsilon}} \frac{h_1^{(p)}(t)\mathrm{d}t}{\sqrt{\cos\hat{\theta} - \cos t}}. \tag{34}$$

Due to the invertibility of Abel's integral operator, Eq. (34) determines $h_1^{(p)}(t)$ uniquely for all $t \in [0, \pi - \hat{\epsilon})$. Using Mehler's integral representation of Legendre polynomials,

$$P_n(\cos t) = \frac{\sqrt{2}}{\pi} \int_0^t \frac{\cos\left[(n + \frac{1}{2})x\right]}{\sqrt{\cos x - \cos t}} \mathrm{d}x, \tag{35}$$

and using the absorbing condition (18b), we show that the Fourier coefficients can be expressed in terms of $h_1^{(p)}(t)$:

$$a_0^{(p)} = \sqrt{2} \int_0^{\pi-\hat{\epsilon}} h_1^{(p)}(t)\mathrm{d}t, \tag{36a}$$

$$a_n^{(p)} = \frac{1}{\sqrt{2}} \int_0^{\pi-\hat{\epsilon}} h_1^{(p)}(t) \big[P_n(\cos t) + P_{n-1}(\cos t)\big] \mathrm{d}t, \quad n \geq 1. \tag{36b}$$

After integration of Eq. (33b) from 0 to x,

$$\sum_{n=1}^{\infty} a_n^{(p)} \sin(nx) = \int_0^x F^{(p)}(u)\mathrm{d}u, \qquad x \in [0, \pi - \hat{\epsilon}), \tag{37}$$

we find that $h_1^{(p)}(t)$ satisfies the relation

$$\int_0^{\pi-\hat{\epsilon}} \mathrm{d}t\ h_1^{(p)}(t) \frac{1}{\sqrt{2}} \sum_{n=1}^{\infty} \left[P_n(\cos t) + P_{n-1}(\cos t)\right] \sin(nx) = \int_0^x F^{(p)}(u)\mathrm{d}u. \tag{38}$$

Using the identity [see Eq. (2. 6. 31) from Ref. [15]]

$$\frac{1}{\sqrt{2}} \sum_{n=1}^{\infty} \big[P_n(\cos t) + P_{n-1}(\cos t)\big] \sin(nx) = \frac{\cos\left(\frac{x}{2}\right) H(x-t)}{\sqrt{\cos t - \cos x}}, \tag{39}$$

where $H(t)$ is the Heaviside distribution, we sum the series in the left-hand side of Eq. (38) to get

$$\int_0^x \frac{h_1^{(p)}(t)\mathrm{d}t}{\sqrt{\cos t-\cos x}} = \frac{1}{\cos\left(\frac{x}{2}\right)}\int_0^x F^{(p)}(u)\mathrm{d}u. \tag{40}$$

The function $h_1^{(p)}(t)$ is determined as the solution of the Abel-type integral equation (40) and reads

$$h_1^{(p)}(t) = \frac{2}{\pi}\frac{d}{dt}\int_0^t \frac{\sin\left(\frac{x}{2}\right)\mathrm{d}x}{\sqrt{\cos x-\cos t}}\left[\int_0^x F^{(p)}(u)\mathrm{d}u\right], \quad t\in[0,\pi-\hat{\epsilon}). \tag{41}$$

Substitution of Eq. (41) into Eqs. (36a) and (36b) leads to the set of equations

$$a_0^{(p)} = \frac{2\sqrt{2}}{\pi}\int_0^{\pi-\hat{\epsilon}}\mathrm{d}x\frac{\sin(x/2)}{\sqrt{\cos x+\cos\epsilon}}\left[\int_0^x F^{(p)}(u)\mathrm{d}u\right], \tag{42a}$$

$$a_n^{(p)} = \frac{\sqrt{2}}{\pi}\int_0^{\pi-\hat{\epsilon}}\mathrm{d}t\left\{\frac{\partial}{\partial t}\int_0^t \mathrm{d}x\frac{\sin(x/2)}{\sqrt{\cos x-\cos t}}\left[\int_0^x F^{(p)}(u)\mathrm{d}u\right]\right\}\left[P_n(\cos t)+P_{n-1}(\cos t)\right], \quad n\geq 1. \tag{42b}$$

From Eq. (31), we see that $F^{(p)}(u)$ is a linear combination of the unknown Fourier coefficients $a_m^{(p)}$, thus Eqs. (42a) and (42b) define a linear system of equations. We proceed by simplifying Eqs. (42a) and (42b) in order to provide explicit relations between the Fourier coefficients.

(i) We first simplify the identity (42a) using the relation

$$2m\alpha_m = \frac{2\sqrt{2}}{\pi}\int_0^{\pi-\hat{\epsilon}}\mathrm{d}x\frac{\sin\left(\frac{x}{2}\right)\sin(mx)}{\sqrt{\cos x+\cos\hat{\epsilon}}}, \qquad m\geq 1. \tag{43}$$

To prove Eq. (43), we express the terms $P_m(\cos\hat{\epsilon})$ and $P_{m-1}(\cos\hat{\epsilon})$ in the definition (27b) of α_m through the Mehler's identity (35).

We substitute the explicit expression for $F^{(p)}(u)$ from Eq. (31) into Eq. (42a). Using the integral representation of α_m from Eqs. (25a) and (43), we obtain

$$a_0^{(p)} = -2\alpha_0\left(\left[\partial_r S_\pi^{(p)}\right]_{|r=1} + \frac{1}{2}\left[\partial_r f_0^{(p)}\right]_{|r=1} a_0^{(p)}\right) + \sum_{m=1}^{\infty} 2m\gamma_m^{(p)}\alpha_m\, a_m^{(p)}. \tag{44}$$

(ii) We now simplify the relation (42b) for $a_n^{(p)}$. Substituting the explicit expression (31) for $F^{(p)}(u)$ into Eq. (42b) leads to the following system of equations

$$a_n^{(p)} = -2\alpha_n\left(\left[\partial_r S_\pi^{(p)}\right]_{|r=1} + \frac{1}{2}\left[\partial_r f_0^{(p)}\right]_{|r=1} a_0^{(p)}\right) + \sum_{m=1}^{\infty} M_{nm}\gamma_m^{(p)} a_m^{(p)}, \quad n\geq 1, \tag{45}$$

where the matrix M_{nm} is

$$M_{nm} = \frac{\sqrt{2}}{\pi}\int_0^{\pi-\hat{\epsilon}}\left[\frac{\partial}{\partial t}\int_0^t \mathrm{d}x\frac{\sin(x/2)\sin(mx)}{\sqrt{\cos x-\cos t}}\right]\left[P_n(\cos t)+P_{n-1}(\cos t)\right] \qquad n\geq 1, \quad m\geq 1. \tag{46}$$

We show in Appendix A 3 that the expression for M_{nm} can be simplified into

$$M_{nm} = \frac{m}{2}\int_{-\cos(\hat{\epsilon})}^1 \frac{1}{1+x}\left[P_m(x)+P_{m-1}(x)\right]\left[P_n(x)+P_{n-1}(x)\right]\mathrm{d}x, \qquad n\geq 1, \quad m\geq 1. \tag{47}$$

Interestingly, the set of coefficients α_n is invariant under the action of M: $M\cdot\alpha=\alpha$ (see Appendix A 3).

(iii) We now write explicitly the system of equations on $a_n^{(p)}$. We first define the set of coefficients $(\widetilde{a}_n^{(p)})$ defined through the following matrix inversion:

$$\widetilde{a}_n^{(p)} \equiv \left[\left(I-M\gamma^{(p)}\right)^{-1}\alpha\right]_n, \qquad n\geq 1, \tag{48}$$

where I stands for the identity matrix, and $\gamma^{(p)}$ is a diagonal matrix formed by $\gamma_n^{(p)}$. For an angular sector and $p=0$, one has $\gamma^{(0)}=0$ and retrieves the expected identity $\widetilde{a}_n^{(0)}=\alpha_n$. From Eq. (45), we have

$$a_n^{(p)} = -2\widetilde{a}_n^{(p)}\left(\left[\partial_r S_\pi^{(p)}\right]_{|r=1} + \frac{1}{2}\left[\partial_r f_0^{(p)}\right]_{|r=1} a_0^{(p)}\right), \qquad n\geq 1. \tag{49}$$

Substituting Eq. (49) into Eq. (44) we obtain a closed system of linear equations for $a_0^{(p)}$:

$$\begin{aligned} a_0^{(p)}\left(1+\left[\partial_r f_0^{(p)}\right]_{|r=1}\alpha_0\right) &= -2\left[\partial_r S_\pi^{(p)}\right]_{|r=1}\alpha_0 \\ &\quad -\left(\left[\partial_r S_\pi^{(p)}\right]_{|r=1} + \frac{1}{2}\left[\partial_r f_0^{(p)}\right]_{|r=1} a_0^{(p)}\right)\left(\sum_{m=1}^{\infty} 4m\alpha_m\ \widetilde{a}_m^{(p)}\ \gamma_m^{(p)}\right). \end{aligned} \tag{50}$$

Introducing

$$\mathcal{C}^{(p)} \equiv \alpha_0 + \sum_{m=1}^{\infty} 2m\alpha_m\ \widetilde{a}_m^{(p)}\ \gamma_m^{(p)}, \tag{51}$$

the Fourier coefficients of the Laplace transform of the survival probability take the compact exact form:

$$a_0^{(p)} = \mathcal{C}^{(p)}\left\{\frac{-2\left[\partial_r S_\pi^{(p)}\right]_{|r=1}}{1+\mathcal{C}^{(p)}\left[\partial_r f_0^{(p)}\right]_{|r=1}}\right\}, \tag{52a}$$

$$a_n^{(p)} = \widetilde{a}_n^{(p)}\left\{\frac{-2\left[\partial_r S_\pi^{(p)}\right]_{|r=1}}{1+\mathcal{C}^{(p)}\left[\partial_r f_0^{(p)}\right]_{|r=1}}\right\}, \qquad n\geq 1. \tag{52b}$$

This solution depends on the coefficients $\widetilde{a}_n^{(p)}$ given by Eq. (48). The numerical implementation of the solution from Eqs. (52a) and (52b) requires the truncation of the matrix M involved in Eq. (48) to a finite size $N\times N$. In spite of the truncation, we will refer to the results obtained by this numerical procedure as exact solutions, as their accuracy can be arbitrarily improved by increasing the truncation size N (we checked numerically that the truncation errors decay very rapidly with N). In practice, we set $N=100$.

In the next section, we propose an approximate expression for the Fourier coefficients $a_n^{(p)}$ which does not rely on a matrix inversion.

3. Approximate resolution scheme

The obtention of an approximate solution, which provides a concise and explicit expression for the FPT, is one of the main result of this paper. The idea of the approximate solution is to substitute the matrix M by the identity matrix in Eq. (48). In Refs. [31, 32] and [33], such a substitution was shown to be efficient to compute the MFPT of a particle alternating phases of surface and bulk diffusions in a spherically symmetric domain.

The substitution of the matrix M by the identity matrix is exact for $\epsilon=0$ as the asymptotic expansion of M_{nm} in the limit $\epsilon\ll 1$ reads (see Appendix A 4)

$$M_{nm} = \delta_{nm} + \frac{nm^2(-1)^{n+m}}{8}\hat{\epsilon}^4 + \mathcal{O}(\hat{\epsilon}^5), \qquad n\geq 1, \quad m\geq 1, \tag{53}$$

where δ_{nm} is the Kronecker symbol. The approximation $M_{nm}=\delta_{nm}$ allows one to invert the matrix in Eq. (48), yielding the following approximate solution:

$$\widetilde{a}_n^{(p)} \approx \frac{\alpha_n}{1-\gamma_n^{(p)}}. \tag{54}$$

Within the approximate scheme, we define

$$\mathcal{C}_a^{(p)} \equiv \alpha_0 + \sum_{m=1}^{\infty} \frac{2m\alpha_m^2 \gamma_m^{(p)}}{1-\gamma_m^{(p)}}, \tag{55}$$

and then substitute $\mathcal{C}^{(p)}$ by $\mathcal{C}_a^{(p)}$ in Eqs. (52a) and (52b). Numerical simulations indicate a $\mathcal{O}(\hat{\epsilon})$ discrepancy between the approximate and the exact solutions. Note that the approximate solution is also exact in the limit $\hat{\epsilon} = \pi$, as it predicts $\alpha_n = 0$ for all $n \geq 0$.

In the next section, we test the accuracy of the approximate expression for the FPT distribution in the disk. We show that the approximate expression describes accurately the exact FPT distribution for any value of $\hat{\epsilon}$ between 0 and π.

C. Results for the disk

In this section, we focus on the FPT distribution for a Brownian particle confined in the disk (Fig. 1(a)).

1. *Short–time and long–time behaviour of the distribution of exit time*

Figures 2 and 3 show the exact and approximate FPT probability densities that are computed through the inverse Laplace transform of $\rho^{(p)}(r,\theta)$ from Eqs. (9), (52a) and (52b). The exact and approximate solutions agree well with the numerical results which are obtained by two independent techniques: (i) a finite element method (FEM) resolution of Eqs. (6a – 6d) in the time domain by COMSOL [34], and (ii) Monte Carlo simulations of a large sample of random walks (see Appendix D for further information on these computational techniques). In both numerical solutions, the problem is solved in time domain, i.e., without Laplace transform inversion. Even for a large exit size $\epsilon = \pi/4$, the approximate solution from Sec. II B 3 agrees well with both the exact solution and the numerical results (see Fig. 2). The agreement is improved uniformly in time for smaller values of ϵ (Fig. 3).

The time scale R^2/D separates the short-time and the long-time behaviors of the FPT distribution, as illustrated on Figs. 2(a–b). In addition, Fig. 2(c) shows the diffusive propagator $\tilde{G}^{(t)}(\vec{r}_0, \vec{r})$ as a function of the arrival position $\vec{r}$ (computed by a finite element method in COMSOL). The spatial distribution of the diffusive propagator provides the following physical insight on the evolution of the FPT in the short-time (i) and long-time regimes (ii):

(i) For $t \ll R^2/D$, most particles do not have enough time to reach the confining boundary (*a fortiori* the exit) and the confining domain appears to be almost infinite. This can be seen on the profile of the diffusive propagator for $t < 1$ in Fig. 2(c). If the distance x_0 from the initial position (r,θ) to the center of the exit $(1,\pi)$, $x_0(r,\theta) = \sqrt{1+r^2-2r\cos(\theta)}$, is sufficiently small (e.g., for $(r,\theta) = (0.25,\pi)$ in Fig. 2), the short-time behavior of the FPT probability density is approximatively

$$\tilde{\rho}^{(t)}(r,\theta) \approx \frac{x_0(r,\theta)}{\sqrt{4\pi D t^3}} \exp\left(-\frac{x_0^2(r,\theta)}{4Dt}\right), \tag{56}$$

which describes the FPT for a particle started at distance x_0 from the absorbing endpoint of a semi-infinite segment [1]. The exponential factor strongly dominates at short times when $\sqrt{4Dt} \ll x_0(r,\theta)$. At the intermediate times, when $x_0(r,\theta) \ll \sqrt{4Dt} \ll R$, the FPT probability density exhibits a power law decay, $\tilde{\rho} \propto t^{-\beta}$, with $\beta = 3/2$. For a starting position $(r,\theta) = (0.90,\pi)$, a fit of the FPT probability density at the intermediate times $t \in [0.1, 0.7]$ by a power law distribution $t^{-\beta}$ yields $\beta = 1.49 \pm 0.02$, a value which is close to the corresponding value of β in a semi-infinite system ($\beta = 1.50$, see Eq. (56)).

(ii) For $t \gg R^2/D$, the FPT probability density exhibits an exponential tail. The terms in braces in Eqs. (52a) and (52b) determine the decay rate of the exponential tail. Note that in Fig. 2 the rescaled profile of the diffusive propagator appears stationary for all $t > R^2/D = 1$, as expected.

The survival probability $\tilde{S}^{(t)}$ (resp. the FPT probability density $\tilde{\rho}^{(t)}$) can be expressed as the sum over the residues of the Laplace transform $S^{(p)}$ (resp. $\rho^{(p)}$). For example, if the boundary is fully absorbing

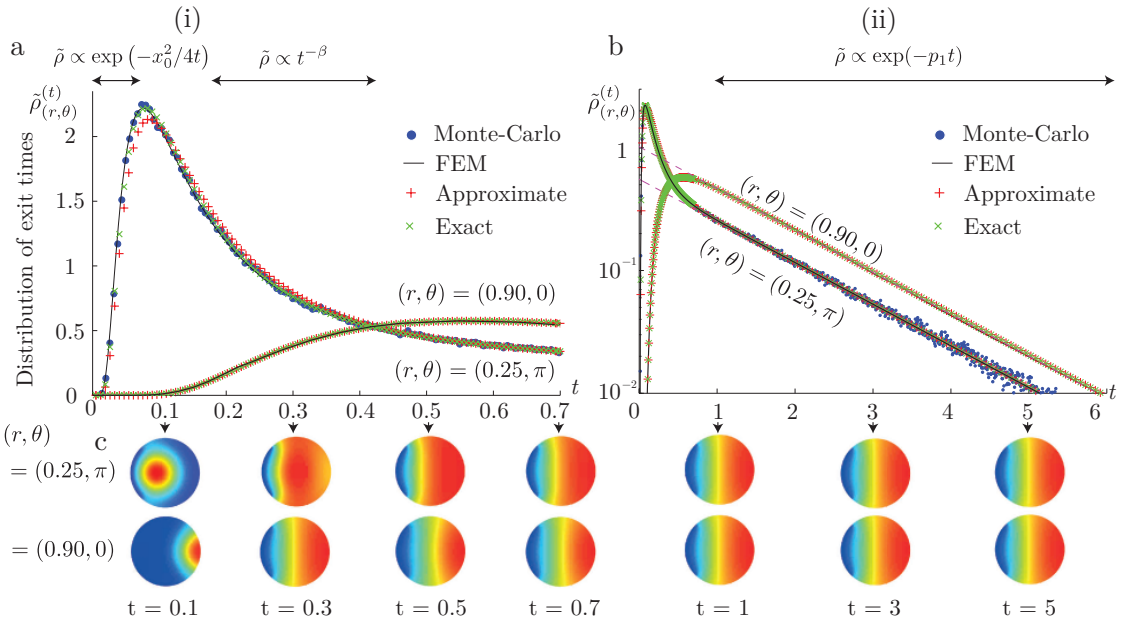

FIG. 2: (Color Online) **Upper panel**: The probability density of the FPT to exit the unit disk through an aperture of half-width $\epsilon = \pi/4$ (Fig. 1) for Brownian particles started at $(r,\theta) = (0.25, \pi)$ and $(r,\theta) = (0.90, 0)$. The probability density is plotted on (**a**) linear scale for $t \in [0, 0.7]$ and (**b**) log-linear scale for $t \in [0, 6]$. The exact solution from Eqs. (52a) and (52b) (green crosses) is compared to the approximate solution from Sec. II B 3 (red pluses), finite element method (solid black line), and Monte Carlo simulations (blue circles) (see Appendix D). **Lower panel**: (**c**) Diffusive propagator $\tilde{G}^{(t)}(\vec{r}_0, \vec{r})$ computed by a FEM at times $t = 0.1, 0.3, 0.5, 0.7, 1, 3, 5$ for the initial positions $(r,\theta) = (0.25, \pi)$ (top row) and $(r,\theta) = (0.90, 0)$ (bottom row). Color changes from dark red to dark blue correspond to changes of the diffusive propagator from large to small values. The FPT probability density remains close to zero during the time needed for the diffusive propagator to spread to the exit. After a time $t > R^2/D = 1$, (i) the diffusive propagator reaches a steady state profile, and (ii) the FPT is close to an exponential distribution with the decay rate constant p_1 predicted by Eq. (58) and shown by magenta dashed lines in **(b)**.

(i.e., $\epsilon = \pi$), the survival probability of a particle started at (r,θ) can be written from Eq. (17). Indeed, after a spectral decomposition of the Laplace operator with Dirichlet boundary condition on the disk [29], the coefficients can be computed from the residue theorem applied to Eq. (17), leading to:

$$\tilde{S}^{(t)}(r,\theta) = \sum_{k=1}^{\infty} \frac{2}{\xi_{0k}} \frac{J_0\left(\xi_{0k} r\right)}{J_1\left(\xi_{0k}\right)} \exp\left(-\xi_{0k}^2 t\right), \tag{57}$$

where the coefficients $-\xi_{0k}$ are the poles of $S_\pi^{(p)}(r)$ (as a function of p), as the coefficients ξ_{0k} are the zeros of the zeroth order Bessel function: $J_0(\xi_{0k}) = 0$ for all $k \geq 1$. Note that the functions $S^{(p)}$ and $\rho^{(p)}$ are related through Eq. (9) and therefore have the same poles. In the general case $\epsilon < \pi$, the long-time behavior of the FPT probability density is governed by the smallest decay rate p_1: $\tilde{\rho}_\pi^{(t)}(r)$ asymptotically decays as $\exp(-p_1 t)$ for $t \gg R^2/D$. The quantity $-p_1$ is the largest negative root of the equation

$$1 + \mathcal{C}^{(p_1)} \left[\partial_r f_0^{(p_1)}\right]_{|r=1} = 0. \tag{58}$$

The latter equation (58) uniquely determines p_1 and can be solved numerically (see Fig. 4). Note that Eq. (58) is independent of the starting position of the particle: in the long-time limit, particles have lost memory of their starting positions. In the next section, we provide explicit estimates of p_1, which yield the long time asymptotics of the FPT distribution in the narrow-escape limit $\epsilon \ll 1$ and beyond.

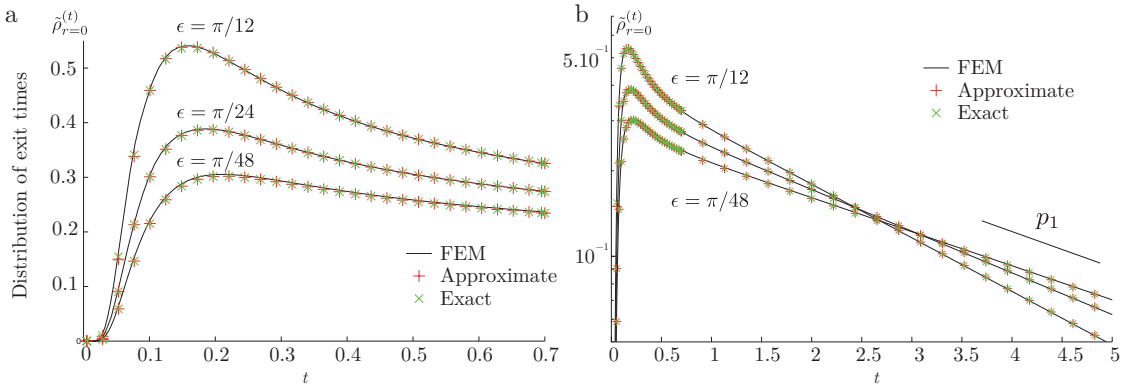

FIG. 3: (Color Online) The FPT probability density for a disk with an exit of half-width $\epsilon = \pi/12, \pi/24, \pi/48$ for Brownian particles started at $r = 0$, in (**a**) linear scale for $t \in [0, 0.7]$, and (**b**) log-linear scale for $t \in [0, 5]$. The exact solution from Eqs. (52a – 52b) (green crosses) is compared to its analytical approximation from Sec. II B 3 (red pluses), and a finite element method resolution (black solid line), showing an excellent agreement (units: $R^2/D = 1$).

2. *Beyond the narrow–escape limit: a simplified expression for the long-time decay rate*

The determination of the FPT distribution for arbitrary ϵ presented above is the main result of the present paper. In this paragraph we first compare our result to the previously known results on the FPT distribution in the narrow–escape limit from Ref. [12]. We then propose a simplified expression for p_1 which does not depend on the specific shape of the domain Ω. This simplified expression is asymptotically exact in the limit $\epsilon \ll 1$ and is in fact in good agreement with the exact expression for p_1 (computed through Eq. (58)) over the whole range of value of ϵ (see Fig. 4).

We first point out that at the first order in $\epsilon \ll 1$, Eqs. (27a) and (27b) read

$$\alpha_0 = 2 \ln \left(\frac{2\phi}{\pi \epsilon} \right) + \mathcal{O}\left(\left(\frac{\epsilon \pi}{\phi} \right)^2 \right), \tag{59a}$$

$$\alpha_n = \frac{(-1)^{n-1}}{n} + \mathcal{O}\left(\left(\frac{\epsilon \pi}{\phi} \right)^2 \right), \qquad n \geq 1. \tag{59b}$$

The logarithmic singularity of Eq. (59a) is a well-known result discussed in Ref. [8] for $\phi = \pi$ and in Ref. [9] for $\phi < \pi$.

In this limit $\epsilon \ll 1$ and if the starting position $\vec{r}$ is located away from the frontier of the confining domain Ω, it has been shown in Ref. [12] that the FPT converges to an exponential distribution with mean the GMFPT $\overline{\mathbb{E}[\tau]}$, defined in Eq. (13). Hence Ref. [12] implies the asymptotic identity: $p_1 = 1/\overline{\mathbb{E}[\tau]}$, for $\epsilon \ll 1$. Due to the divergence of α_0 from Eq. (59a), the latter identity is equivalent to:

$$p_1 = \frac{\pi}{|\Omega|} \frac{2}{\alpha_0}, \quad \forall \epsilon \ll 1. \tag{60}$$

where $|\Omega|$ stands for the volume of Ω. We stress that the latter expression in Eq. (60) depends on $|\Omega|$, but not on the precise shape of the domain Ω. This statement holds however only in the limit $\epsilon \ll 1$, since the exact result of Eq. (58), which is valid for any ϵ, depends a priori on the specific geometry of the domain through the set $(\gamma_m^{(p)})$ in the expression of $C^{(p)}$ (see Eq. (51)).

In fact one can propose a simple approximate expression for p_1 with larger range of validity in ϵ than the asymptotic relation from Eq. (60). Let us first notice that at the leading order in $\epsilon \ll 1$, $\mathcal{C}^{(p)} \approx \alpha_0$. The latter identity leads us to substitution $\mathcal{C}^{(p)}$ for α_0 in Eq. (58). Setting $q_1 = i\sqrt{p_1}$, the simplified expression of Eq. (58) is reduced to:

$$\left[\partial_r f_0^{(q_1)} \right]_{|r=1} \approx \frac{\pi}{|\Omega|} \frac{1}{q_1 \alpha_0}. \tag{61}$$

In the limit $\epsilon \ll 1$, the simplified expression of Eq. (61) leads to the perturbative result of Eq. (60). Note that the simplified expression of Eq. (61) is also exact for $\epsilon = \pi$, in which case α_0 tends to zero and p_1 tends to ξ_{01}^2, in agreement with Eq. (57).

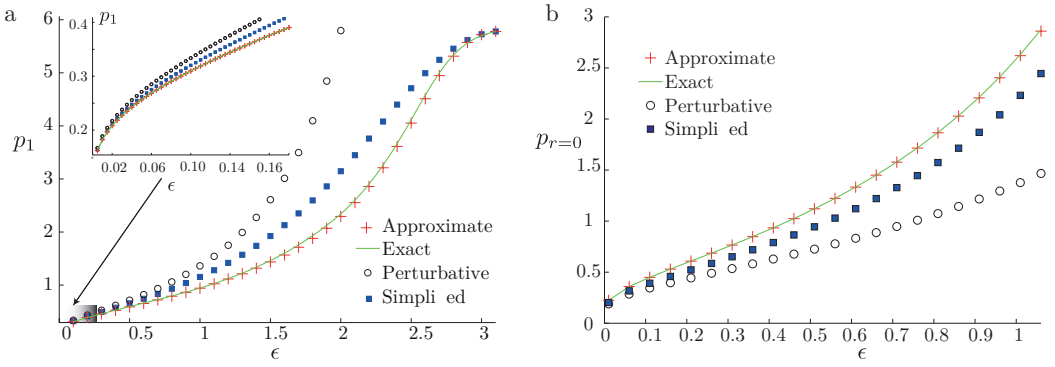

FIG. 4: (Color Online) Comparison of three approximate schemes describing the long-time behavior of the survival probability for a Brownian particle started at $r = 0$ which exits a confining disk through an exit of half-width ϵ. The quantities $p_{r=0}$ and p_1 are defined from the asymptotic expansion: $\log(\tilde{\rho}^{(t)}(r=0)) \simeq \log(p_{r=0}) - p_1 t$ according to Eq. (63). **(a)** Decay rate p_1 of the long-time limit of the survival probability as a function of the exit half-width ϵ. The rate p_1 is obtained through: an exponential interpolation of the exact distribution from Eqs. (52a) and (52b) (solid green line), an exponential interpolation of the approximate distribution from Sec. II B 3 (red pluses), the asymptotic expression $p_1 = 2/\alpha_0$ in the limit $\epsilon \ll 1$ [12] (black circles), and simplified Eq. (61) (blue squares). Note that Eq. (61) provides accurate results in both limits $\epsilon = 0$ and $\epsilon = \pi$, and is more accurate than the perturbative expansion. **(b)** The prefactor $p_{r=0}$ to the exponential distribution defined in Eq. (63) as a function of the exit half-width ϵ.

Finally, for a given value of the decay rate p_1, the residue theorem leads to the following long-time exponential decay of the survival probability:

$$\tilde{S}^{(t)}(r,\theta) \approx \left(-2\left[\partial_r S_\pi^{(p_1)}\right]_{|r=1}\right)\left[\frac{J_0\left(\sqrt{p_1}r\right)}{J_0\left(\sqrt{p_1}\right)}\frac{\alpha_0}{2} + \sum_{m=1}^{\infty}\frac{J_m\left(\sqrt{p_1}r\right)}{J_m\left(\sqrt{p_1}\right)}\alpha_m \cos\left(\frac{m\theta\phi}{\pi}\right)\right]\exp\left(-p_1 t\right) \tag{62}$$

$$\approx p_{(r,\theta)}\exp\left(-p_1 t\right), \tag{63}$$

where $p_{(r,\theta)}$ is the prefactor of the exponential distribution, which depends on the starting position $X(0) = (r,\theta)$. In Fig. 4, we show that the simplified solution of Eq. (61) provides a good approximation of p_1 over the whole range of values for ϵ.

D. Moments and cumulants

In this section we derive exact expressions for the moments of the exit times for a general set of functions $f_n^{(p)}$, $n \geq 0$. We emphasize that these expressions are fully explicit in the case of Brownian particles confined in an angular sector.

We use the notations $a_n^{[k]}$ for the k-th coefficient in the small $p \ll 1$ expansion of $a_n^{(p)}$:

$$a_n^{(p)} \equiv \sum_{k=0}^{\infty} p^k a_n^{[k]}, \qquad n \geq 0. \tag{64}$$

By definition $a_n^{(0)} = a_n^{[0]}$. Similarly we define for all $k \geq 0$ the set of coefficients $S^{[k]}(r,\theta)$, $\left[\partial_r S_\pi^{[k]}\right]_{|r=1}$, $\left[\partial_r f_0^{[k]}\right]_{|r=1}$, $f_n^{[k]}$, and $\gamma_n^{[k]}$ for all $n \geq 0$. From Eqs. (16) and (19), the coefficient $S^{[j]}(r,\theta)$ is given in terms of $a_0^{[j]}$, $j \geq 0$:

$$S^{[j]}(r,\theta) = S_\pi^{[j]}(r) + \sum_{k=0}^{j}\frac{a_0^{[k]}}{2} f_0^{[j-k]}(r) + \sum_{n=1}^{\infty}\left(\sum_{k=0}^{j} a_n^{[k]} f_n^{[j-k]}(r)\right)\cos\left(\frac{n\pi\theta}{\phi}\right). \tag{65}$$

In the next section, we explain how the coefficients $a_n^{[j]}$ can be expressed through the lower-order terms $a_n^{[k]}, 0 \leq k \leq j-1$.

1. Recurrence relation on the Fourier coefficients

We show that the Fourier coefficients satisfy a hierarchical set of equations, i.e., it is possible to express $a_n^{[j]}$ in terms of the lower-order coefficients $a_n^{[k]}, n \geq 0$, with $k = 0, 1, \ldots, j-1$. The Fourier coefficients of the MFPT are obtained by setting $p = 0$ in Eqs. (52a) and (52b):

$$\mathbb{E}\left[\tau_{(r,\theta)}\right] = S_\pi^{(0)}(r) + \frac{a_0^{(0)}}{2} f_0^{(0)}(r) + \sum_{n=1}^{\infty} a_n^{(0)} f_n^{(0)}(r) \cos\left(\frac{n\pi\theta}{\phi}\right), \qquad (r,\theta) \in \Omega. \tag{66}$$

For instance, one retrieves the exact explicit expression (28) for the MFPT of Brownian particles confined in an angular sector. In other geometries considered in Sec. III, the exact resolution scheme requires a numerical solution of linear Eqs. (48) at $p = 0$.

According to Eq. (45), the unknown coefficients $a_n^{[j]}$ are related to the unknown coefficients $a_0^{[j]}$ and to the known lower-order coefficients $a_n^{[k]}$, $k = 1, 2, \ldots, j-1$,

$$\sum_{m=1}^{\infty} (\delta_{nm} - M_{nm}\gamma_m^{[0]}) a_m^{[j]} = -2\alpha_n \left(\left[\partial_r S_\pi^{[j]}\right]_{|r=1} + \frac{1}{2} \sum_{k=0}^{j} a_0^{[j-k]} \left[\partial_r f_0^{[k]}\right]_{|r=1} \right) + \sum_{m=1}^{\infty} M_{nm} \left(\sum_{k=1}^{j} \gamma_m^{[k]} a_m^{[j-k]} \right). \tag{67}$$

In terms of the vector $\widetilde{\alpha}_n^{(0)}$ defined by Eq. (48) with $p = 0$, the matrix $\widetilde{M}$ is defined as

$$\widetilde{M} \equiv (I - M \cdot \gamma^{(0)})^{-1} \cdot M. \tag{68}$$

where I stands for the identity matrix, and $\gamma^{(0)}$ is a diagonal matrix formed by $\gamma_n^{(0)}$. In terms of the matrix $\widetilde{M}$, Eq. (67) takes the form

$$a_n^{[j]} = -2\widetilde{\alpha}_n^{(0)} \left(\left[\partial_r S_\pi^{[j]}\right]_{|r=1} + \frac{1}{2} \sum_{k=0}^{j} a_0^{[j-k]} \left[\partial_r f_0^{[k]}\right]_{|r=1} \right) + \sum_{m=1}^{\infty} \widetilde{M}_{nm} \left(\sum_{k=1}^{j} \gamma_m^{[k]} a_m^{[j-k]} \right). \tag{69}$$

Substituting this expression into Eq. (44) leads to

$$a_0^{[j]} = \frac{-2\alpha_0 \left(\left[\partial_r S_\pi^{[j]}\right]_{|r=1} + \frac{1}{2} \sum_{k=1}^{j} a_0^{[j-k]} \left[\partial_r f_0^{[k]}\right]_{|r=1} \right) + \sum_{m=1}^{\infty} 2m\alpha_m T_m^{[j]}}{1 + \left[\partial_r f_0^{[0]}\right]_{|r=1} \left(\alpha_0 + \sum_{m=1}^{\infty} 2m\alpha_m \widetilde{\alpha}_m^{(0)} \gamma_m^{[0]} \right)}, \tag{70}$$

where

$$T_m^{[j]} = \sum_{k=1}^{j} \gamma_m^{[k]} a_m^{[j-k]} + \gamma_m^{(0)} \left[-2\widetilde{\alpha}_m^{(0)} \left(\left[\partial_r S_\pi^{[j]}\right]_{|r=1} + \frac{1}{2} \sum_{k=0}^{j} a_0^{[j-k]} \left[\partial_r f_0^{[k]}\right]_{|r=1} \right) + \sum_{l=1}^{\infty} \widetilde{M}_{ml} \left(\sum_{k=1}^{j} \gamma_l^{[k]} a_l^{[j-k]} \right) \right]. \tag{71}$$

Equation (70) expresses $a_0^{[j]}$ in terms of the known coefficients $a_n^{[k]}$, $k = 1, 2, \ldots, j-1$. The coefficients $a_n^{[j]}$ ($n \geq 1$) are then determined through Eq. (69).

Following the idea of Sec. II B, we define an approximate scheme in which the matrix M is replaced by the identity matrix in Eqs. (52a), (52b) and (68). This approximation leads to Eq. (54) and solves Eq. (68) as

$$\widetilde{M}_{nm} \approx \frac{M_{nm}}{1 - \gamma_n^{(0)}}. \tag{72}$$

We recall that the approximation $M_{mn} = \delta_{mn}$ is exact in the limit $\epsilon = 0$ (see Eq. (53)).

In the next section, we focus on Brownian particles confined in an angular sector, in which case the recursive method of Eq. (70) provides an exact explicit expression for the variance and an exact computation scheme of the third and fourth moments.

2. Diffusion in angular sector: explicit exact moments

For Brownian particles confined in an angular sector, the coefficients $\gamma_n^{(0)}$ are equal to zero. The recursive scheme provides thus an exact explicit expression for the moments of the exit time as the resolution of Eqs. (48) and (68) is straightforward. Following the method of Sec. II D 1, we obtain the second moment of the exit time by combining Eqs. (28) and (70):

$$\mathbb{E}\left[\tau_{(r,\theta)}^2\right] = \left[\frac{1}{2}\left(\frac{\alpha_0\pi}{\phi}\right)^2 + \frac{1}{8}\left(\frac{\alpha_0\pi}{\phi}\right)(3-2r^2) + \frac{3+r^4-4\,r^2}{32} + \sum_{m=1}^{\infty}\frac{\phi}{m\pi+\phi}\left(\frac{\alpha_m\pi}{\phi}\right)^2\right] + \sum_{n=1}^{\infty}\left[\alpha_n\left(\frac{1}{4}+\alpha_0\frac{\phi}{\pi}+\frac{\phi(1-r^2)}{2(n\pi+\phi)}\right) + \sum_{m=1}^{\infty}\frac{M_{nm}\phi^2}{m\pi(m\pi+\phi)}\alpha_m\right]\frac{\phi\, r^{n\pi/\phi}}{\pi}\cos\left(\frac{n\pi\theta}{\phi}\right). \quad (73)$$

Substracting the square of the MFPT defined in Eq. (28), we obtain the variance of the exit time for any starting position within the angular sector. We point out that the variance was previously known only in the narrow-escape limit $\epsilon \ll 1$ through its leading order term $\alpha_0^2/4$ [12]. Figures 5 and 6 show the standard deviation, defined as the square root of the variance, as a function of the starting position (r,θ) within the disk ($\phi=\pi$) and an angular sector ($\phi=\pi/3$), respectively.

The average of Eq. (73) over all starting positions within the angular sector (defined in Eq. (29)) leads to

$$\overline{\mathbb{E}\left[\tau^2\right]} = \frac{1}{2}\left(\frac{\alpha_0\pi}{\phi}\right)^2 + \frac{1}{4}\left(\frac{\alpha_0\pi}{\phi}\right) + \frac{1}{24} + \sum_{m=1}^{\infty}\frac{1}{m\pi/\phi+1}\left(\frac{\alpha_m\pi}{\phi}\right)^2. \quad (74)$$

On the other hand, the spatial average of Eq. (28) turns out to be

$$\overline{\mathbb{E}\left[\tau\right]}^2 = \frac{1}{2}\overline{\mathbb{E}\left[\tau^2\right]}. \quad (75)$$

Combining these two results, one gets the following expression of the spatial average of the variance:

$$\overline{\mathrm{Var}\left[\tau\right]} = \overline{\mathbb{E}\left[\tau^2\right]} - \overline{\mathbb{E}\left[\tau\right]}^2 = \overline{\mathbb{E}\left[\tau\right]}^2 = \frac{1}{4}\left(\frac{\alpha_0\pi}{\phi}\right)^2 + \frac{1}{8}\left(\frac{\alpha_0\pi}{\phi}\right) + \frac{1}{48} + \frac{1}{2}\sum_{m=1}^{\infty}\frac{1}{m\pi/\phi+1}\left(\frac{\alpha_m\pi}{\phi}\right)^2. \quad (76)$$

The equality between the averaged variance and the averaged second moment, $\overline{\mathrm{Var}\left[\tau\right]} = \overline{\mathbb{E}\left[\tau\right]}^2$, was previously obtained from general arguments [16].

We now consider the random variable τ_Ω, defined as the exit time of a particle started at a random starting position, with uniform distribution within Ω. Although the averaged moments are identical, $\overline{\mathbb{E}\left[\tau^n\right]} = \mathbb{E}\left[\tau_\Omega^n\right]$ (see Appendix B), the variance of τ_Ω,

$$\mathrm{Var}\left[\tau_\Omega\right] = \mathbb{E}\left[\tau_\Omega^2\right] - \mathbb{E}\left[\tau_\Omega\right]^2 = \frac{1}{4}\left(\frac{\alpha_0\pi}{\phi}\right)^2 + \frac{1}{8}\left(\frac{\alpha_0\pi}{\phi}\right) + \frac{5}{192} + \sum_{m=1}^{\infty}\frac{1}{m\pi/\phi+1}\left(\frac{\alpha_m\pi}{\phi}\right)^2. \quad (77)$$

is different from the spatially averaged variance of Eq. (76).

Following the method of Sec. II D 1, we compute the Fourier coefficient of the third moment from the Fourier coefficients of the two first moments. Similarly, we compute the fourth moment from the three first moments. We define the skewness $\mathrm{Ske}\left[\tau_{(r,\theta)}\right]$ and the excess kurtosis $\mathrm{Kur}\left[\tau_{(r,\theta)}\right]$ as

$$\mathrm{Ske}\left[\tau_{(r,\theta)}\right] = \mathbb{E}\left[\left(\frac{\tau-\mathbb{E}\left[\tau\right]}{\sqrt{\mathbb{E}\left[\tau^2\right]-\mathbb{E}\left[\tau\right]^2}}\right)^3\right] \quad \text{and} \quad \mathrm{Kur}\left[\tau_{(r,\theta)}\right] = \mathbb{E}\left[\left(\frac{\tau-\mathbb{E}\left[\tau\right]}{\sqrt{\mathbb{E}\left[\tau^2\right]-\mathbb{E}\left[\tau\right]^2}}\right)^4\right] - 3. \quad (78)$$

Figures 5 and 6 show the skewness and the excess kurtosis for a Brownian particle confined in a disk and an angular sector, respectively. The lower bounds for the skewness and kurtosis are respectively 2 and 6, e.g. the values of the skewness and excess kurtosis of an exponential distribution. A positive skewness indicates that the distribution of exit times is always skewed to the right of the MFPT. The distribution is also leptokurtic, meaning that the excess kurtosis is positive: very long residence times occur more frequently than predicted by a Gaussian distribution.

The ratio of the standard deviation to the mean, the skewness, and the excess kurtosis diverge when the distance between the starting position and the center of the exit tends to zero. This is consistent with the short-time behavior of the FPT distribution.

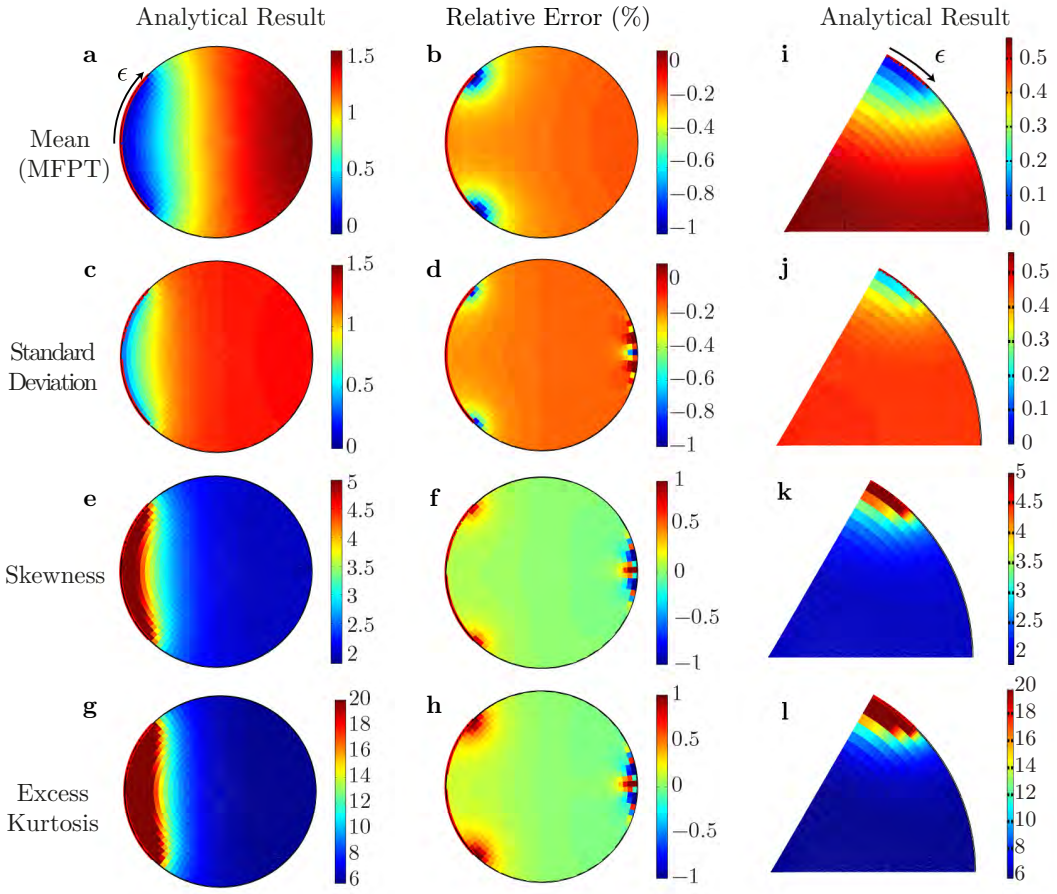

FIG. 5: (Color Online) Mean, variance, skewness and excess kurtosis of the FPT for a Brownian particle confined in: a disk ($\phi = \pi$) with the exit width $2\epsilon = \pi/2$ shown by red line (**left column**), and an angular sector ($\phi = \pi/3$) with an exit at the corner of the width $\epsilon = \phi/4$ shown by red line (**right column**). The middle column (**b-d-f-h**) shows the relative error $(X_n - X_a)/X_n$ between the analytical result X_a and a finite element method resolution X_n. The exit of half-width $\epsilon = \pi/4$ is shown by red line. The relative error for the cumulants is the largest near the edges of the exit. Outside a boundary layer near to the exit, the first four moments are very close to those of an exponential distribution (for which the standard deviation is equal to the mean, while the skewness and excess kurtosis are equal to 2 and 6 respectively).

3. Moments in the narrow-escape limit: the case of the disk

The argument of Ref. [12] holds in the narrow-escape limit $\epsilon \ll 1$ and for a starting position $\vec{r}$ away from the frontier of the confining domain Ω. Under these two assumptions, one expects the set $\left(\mathbb{E}\left[\tau_{(r,\theta)}^n\right]\right), n \geq 1$ to converge to the set $\left(n!\,\mathbb{E}\left[\tau_{(r,\theta)}\right]\right), n \geq 1$ which are the set of moments of an exponential distribution of mean $\mathbb{E}\left[\tau_{(r,\theta)}\right]$.

Figure 6 shows the first four cumulants of the exit time in the case $\epsilon = \pi/60$ in the boundary of an unit disk. Following the argument of Ref. [8], we introduce

$$\delta = -\epsilon \ln\left(\frac{\epsilon}{2}\right), \tag{79}$$

and define the boundary layer $\mathcal{B}[(1,\pi),\delta]$ as the intersection of Ω with the disk of radius 2δ centered on the exit $(r,\theta) = (1,\pi)$ (i.e. the area enclosed by the dashed line in Fig. 6). For a starting position $(r,\theta) \in \Omega\backslash\mathcal{B}[(1,\pi),\delta]$ outside the boundary layer, the ratio of the standard deviation to the MFPT is close to 1, while the skewness and excess kurtosis are respectively close to 2 and 6, as for an exponential distribution. As a consequence, for a sufficiently small exit and for a starting position $(r,\theta) \in \Omega\backslash\mathcal{B}[(1,\pi),\delta]$ outside the boundary layer, the exit time follows approximately an exponential distribution whose mean is the MFPT defined by Eq. (28). This observation extends the predictions of Ref. [12].

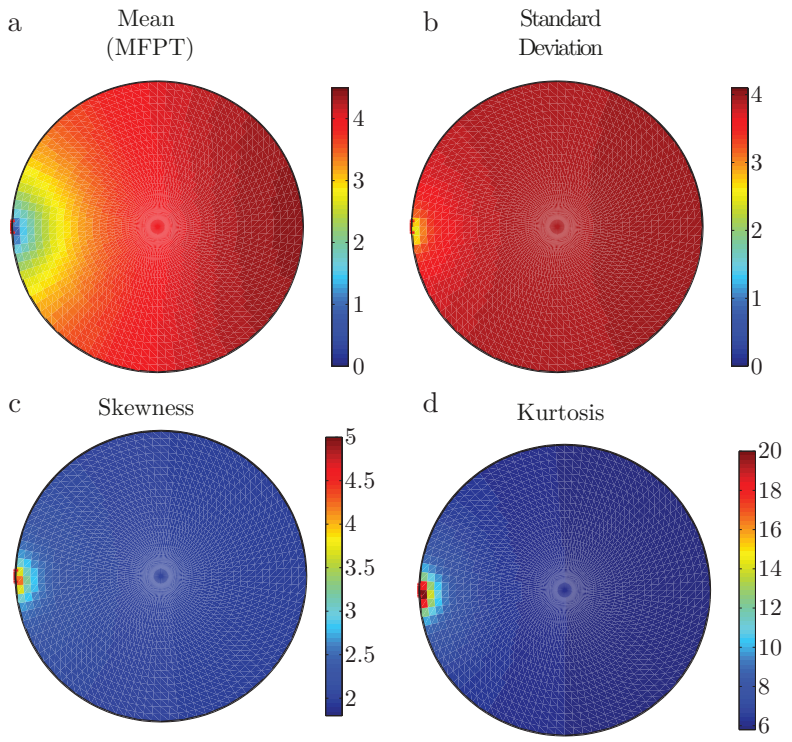

FIG. 6: (Color Online) First four cumulants of the exit time from a disk for $\epsilon = \pi/60$: (**a**) MFPT; (**b**) standard deviation; (**c**) skewness; (**d**) excess kurtosis. The dashed line shows the boundary layer, i.e. the region enclosed within the disk of radius $2\epsilon \ln(\epsilon/2)$. Note that outside the boundary layer, (i) the standard deviation is approximatively equal to the MFPT, and (ii) the skewness and excess kurtosis are approximatively equal to 2 and 6 that correspond to an exponential distribution.

III. EXTENSIONS AND APPLICATIONS

In this section, we discuss various extensions and applications of our approach. First, we apply the general framework of Sec. II to consider the exit time for a Brownian particle from annuli (Sec. III A). Second, we extend the method of Sec. II to obtain the FPT distribution for particles moving according to radial advection-diffusion (Sec. III B). We also show the applicability of this method to the FPT problems in rectangles (III C). Finally, we briefly discuss the analogies of the FPT problem to heat transfer (Sec. III D) and to microchannel flows (Sec. III E). Table II summarizes explicit expressions of the functions $S_\pi^{(p)}(r)$ and $f_n^{(p)}$ for each considered domain. Using Table II to compute the Fourier coefficients in Eqs. (52a) and (52b), one gets the FPT distribution for each considered geometry. In addition, the recursive scheme in Eq. (70) provides all the moments of the exit time.

A. Annuli

We consider the confining domain Ω to be an annulus with concentric circular boundaries at $r = R = 1$ and $r = R_c$: $\Omega = \{(r,\theta) \in \mathbb{R}^2 \ : \ R_c < r < 1, \ 0 \le \theta < 2\pi\}$ for $R_c < 1$ (the exit is located on the outer boundary) or $\Omega = \{(r,\theta) \in \mathbb{R}^2 \ : \ 1 < r < R_c, \ 0 \le \theta < 2\pi\}$ for $R_c > 1$ (the exit is located on the inner boundary). The boundary at $r = R_c$ is fully reflecting, while the boundary at $r = 1$ is reflecting except for an absorbing arc of length 2ϵ, as illustrated in Fig. 8(b). The survival probability in the Laplace space satisfies the Helmholtz Eq. (14a), the mixed Neumann-Dirichlet boundary conditions of Eqs. (14b)-(14c) at $r = 1$ and the Neumann boundary condition at $r = R_c$ from Eq. (14d).

TABLE II: Summary of the quantities involved in the computation of the Laplace transform of the survival probability in five studied geometries. The functions f_n are defined for all $n \geq 0$ while the functions γ_n are defined for all $n \geq 1$.

Case	Quantity	Series expansion in $p \ll 1$
Full disk	$S_\pi^{(p)}(r) = \frac{1}{p}\left(1 - \frac{I_0[\sqrt{p}r]}{I_0[\sqrt{p}]}\right)$	$\frac{1-r^2}{4} + \frac{\left(-3+4r^2-r^4\right)}{64}p + \mathcal{O}(p^2)$
(no bias)	$f_n^{(p)}(r) = \frac{I_n(\sqrt{p}r)}{I_n(\sqrt{p})}$	$r^n\left(1 + \frac{\left(r^2-1\right)p}{4(1+n)}\right) + \mathcal{O}(p^2)$
Sec. II	$\gamma_n^{(p)} = 1 - \frac{\sqrt{p}}{2n}\frac{I_{n-1}(\sqrt{p})+I_{n+1}(\sqrt{p})}{I_n(\sqrt{p})}$	$-\frac{p}{2n(n+1)} + \mathcal{O}(p^2)$
Angular Sector	$S_\pi^{(p)}(r) = \frac{1}{p}\left(1 - \frac{I_0[\sqrt{p}r]}{I_0[\sqrt{p}]}\right)$	$\frac{1-r^2}{4} + \frac{\left(-3+4r^2-r^4\right)}{64}p + \mathcal{O}(p^2)$
of half-width ϕ	$f_n^{(p)}(r) = \frac{\phi}{\pi}\frac{I_{n\pi/\phi}(\sqrt{p}r)}{I_{n\pi/\phi}(\sqrt{p})}$	$\frac{\phi\, r^{\frac{n\pi}{\phi}}}{\pi}\left(1 + \frac{\left(r^2-1\right)\phi p}{4(n\pi+\phi)}\right) + \mathcal{O}(p^2)$
Sec. II	$\gamma_n^{(p)} = 1 - \frac{\sqrt{p}}{2n}\frac{I_{n\pi/\phi-1}(\sqrt{p})+I_{n\pi/\phi+1}(\sqrt{p})}{I_{n\pi/\phi}(\sqrt{p})}$	$-\frac{p\phi}{2n\pi\left(n\frac{\pi}{\phi}+1\right)} + \mathcal{O}(p^2)$
Full Disk	$S_\pi^{(p)}(r) = \frac{1}{p} - \frac{r^{-\frac{\mu}{2}}}{p}\frac{I_{\mu/2}(\sqrt{p}r)}{I_{\mu/2}(\sqrt{p})}$	$(1-r^2)\left(\frac{1}{2(2+\mu)} + p\,\frac{\left(-6-\mu+(2+\mu)r^2\right)}{8(2+\mu)^2(4+\mu)}\right) + \mathcal{O}(p^2)$
with bias:	$f_n^{(p)}(r) = r^{-\frac{\mu}{2}}\frac{I_{\mu_n}(\sqrt{p}r)}{I_{\mu_n}(\sqrt{p})}$	$r^{(\mu_n-\mu)/2}\left(1 + p\,\frac{r^2-1}{2(2+\mu_n)}\right) + \mathcal{O}(p^2)$
$\vec{v}(r) = \frac{\mu D}{r^2}\,\vec{r}$	where $\mu_n = \sqrt{n^2 + \left(\frac{\mu}{2}\right)^2}$	
Sec. III B	$\gamma_n^{(p)} = 1 - \frac{\left[\partial_r f_n^{(p)}\right]_{r=1}}{n}$	$1 + \frac{\mu}{2m} - \sqrt{1+\left(\frac{\mu}{2m}\right)^2} - \frac{p}{2m\left(1+\sqrt{m^2+(\mu/2)^2}\right)}$
Annuli	$\rho_n(\sqrt{p}r) \equiv \frac{I_n[\sqrt{p}r]}{I_n[\sqrt{p}]}, \quad \nu_n(\sqrt{p}r) \equiv \frac{K_n[\sqrt{p}r]}{K_n[\sqrt{p}]}$	
Sec. III B	$S_\pi^{(p)}(r) = \frac{1}{p} - \frac{1}{p}\frac{\rho_0(\sqrt{p}r) - \frac{\rho_0'(\sqrt{p}r)}{\nu_0'(\sqrt{p}R_c)}\nu_0(\sqrt{p}r)}{1-\frac{\rho_0'(\sqrt{p}r)}{\nu_0'(\sqrt{p}R_c)}}$	$\frac{1}{4}\left(1 - r^2 + 2R_c^2\log(r)\right) + \mathcal{O}(p)$
	$f_n^{(p)}(r) = \frac{\rho_n(\sqrt{p}r) - \frac{\rho_n'(\sqrt{p}R_c)}{\nu_n'(\sqrt{p}R_c)}\nu_n(\sqrt{p}r)}{1-\frac{\rho_n'(\sqrt{p}R_c)}{\nu_n'(\sqrt{p}R_c)}}$	$\frac{r^{2n}+Rc^{2n}}{r^n(1+Rc^{2n})} + \mathcal{O}(p^2)$
	$\gamma_n^{(p)} = 1 - \frac{\left[\partial_r f_n^{(p)}\right]_{r=1}}{n}$	$\frac{2Rc^{2n}}{1+Rc^{2n}} + \mathcal{O}(p)$
Rectangle	$S_\pi^{(p)}(r) = \frac{1}{p}\left(1 - \frac{\cosh(\sqrt{p}r)}{\cosh\left(\sqrt{p}R\right)}\right)$	$\frac{R^2-r^2}{2} + \frac{1}{24}\left(-r^4 + 6r^2R^2 - 5R^4\right)p + \mathcal{O}(p^2)$
of width $\phi = \pi$	$f_n^{(p)}(r) = \frac{\cosh\left(\sqrt{p+n^2}\ r\right)}{\cosh(\sqrt{p+n^2}R)}$	$\frac{\cosh(nr)}{\cosh(nR)} + \mathcal{O}(p)$
Sec. III C	$\gamma_n^{(p)} = 1 - \frac{\sqrt{p+n^2}\tanh\left(\sqrt{p}R\right)}{n}$	$(1-\tanh(nR)) - \frac{\left(\frac{nR}{\cosh(nR)^2} + \tanh(nR)\right)p}{2n^2} + \mathcal{O}(p^2)$

1. *Distribution of the first passage time*

In Fig. 7 we represent the FPT probability density $\tilde{\rho}^{(t)}(r,\theta)$ for an annulus with $R_c = 0.70$ and an exit of half-size $\epsilon = \pi/24$, with three starting positions: $(r,\theta) = (0.90,\pi)$, $(0.90,\pi/2)$, and $(0.90,0)$. The exact, approximate and numerical schemes agree well in the whole range of times.

The short-time behavior of the FPT distribution strongly depends on the initial position of the particle. If the starting position is far from the exit [e.g. $(r,\theta) = (0.90,0)$], the FPT probability density is negligible up to time $t \approx R^2/D = 1$. For a starting position that is within the boundary layer defined in Sec. II D 2 [e.g. $(r,\theta) = (0.90,\pi)$], the FPT probability density is sharply picked at $t \approx x_0^2/D = 1$, where x_0 is the distance to the center of the exit. In contrast, the long-time behavior ($t \gg R^2/D$) of the FPT probability density is independent of the initial position.

In the next section, we obtain an explicit approximate expression for the MFPT. Using this approximate expression we find that the MFPT is an optimizable function of R_c under analytically determined criteria.

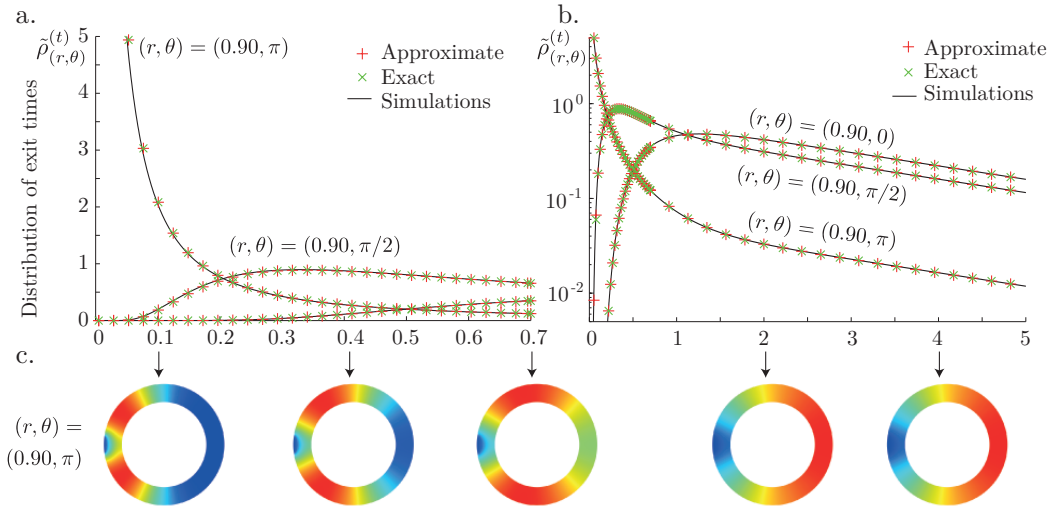

FIG. 7: (Color Online) **Upper panel**: The probability density of the FPT to exit an annulus between two circles of radii $R_c = 0.7$ and $R = 1$ through an exit of half-width $\epsilon = \pi/24 \approx 0.13$ within the outer radius R, for a Brownian particle started at $(r,\theta) = (0.90, \pi), (0.90, \pi/2), (0.90, 0)$. The FPT probability density is shown in (**a**) linear scale for $t \in [0, 0.7]$, and (**b**) log-linear scale for $t \in [0, 6]$. The exact solution from Eqs. (52a) and (52b) (green crosses) is compared to its analytical approximation from Sec. II B 3 (red pluses) and a finite element method numerical solution (black solid line). **Lower panel**: Diffusive propagator $\tilde{G}^{(t)}(\vec{r}_0, \vec{r})$ computed by a FEM at times $t = 0.1, 0.4, 0.7, 2, 4$ for the initial position $(r,\theta) = (0.90, \pi)$. Color changes from dark red to dark blue correspond to changes of the diffusive propagator from large to small values. After a time $t > R^2/D = 1$, the diffusive propagator reaches a steady state profile, and the FPT distribution agrees well with an exponential distribution with the decay rate constant p_1.

2. *Approximate expression for the MFPT*

We substitute $\mathcal{C}^{(0)}$ by $\mathcal{C}_a^{(0)}$ from Eq. (55) into Eqs. (52a) and (52b) and use the expressions of Table II to get the following approximation for the Fourier coefficients of the MFPT:

$$a_0^{(0)} \approx \left(1 - R_c^2\right) \left[\alpha_0 + \sum_{k=1}^{\infty} \left(\frac{2R_c^{2k}}{R_c^{2k} - 1}\right) 2k\alpha_k^2\right], \tag{80}$$

$$a_n^{(0)} \approx \left(1 + R_c^{2n}\right) \frac{1 - R_c^2}{1 - R_c^{2n}} \alpha_n, \quad n \geq 1, \tag{81}$$

where α_n are defined by Eqs. (27b). Using Eqs. (80) and (81), the MFPT can be computed from Eq. (66). The GMFPT defined in Eq. (13) is

$$\overline{\mathbb{E}[\tau]} \approx \frac{1 - R_c^2}{2} \left[\alpha_0 + \sum_{k=1}^{\infty} \left(\frac{R_c^{2k}}{R_c^{2k} - 1}\right) 4k\alpha_k^2\right] + \frac{1}{8}\left(1 - 3R_c^2\right) + \frac{1}{2} \frac{R_c^4 \ln(R_c)}{R_c^2 - 1}. \tag{82}$$

Notice that for $R_c = 0$, we retrieve the exact Eqs. (28) and (29). Let us now compare the approximate solution to previously known results in two limits $R_c \to 1$ and $R_c \gg 1$. This comparison provides an error estimate of the approximate solution in the limit $\epsilon \ll 1$.

(i) In the limit $R_c \to 1$, using the identity

$$\sum_{m=1}^{\infty} 2m\alpha_m^2 = \alpha_0, \tag{83}$$

which is valid for any value of ϵ (and proved in Appendix A 5), we show that the coefficients $a_n^{(0)}$ from

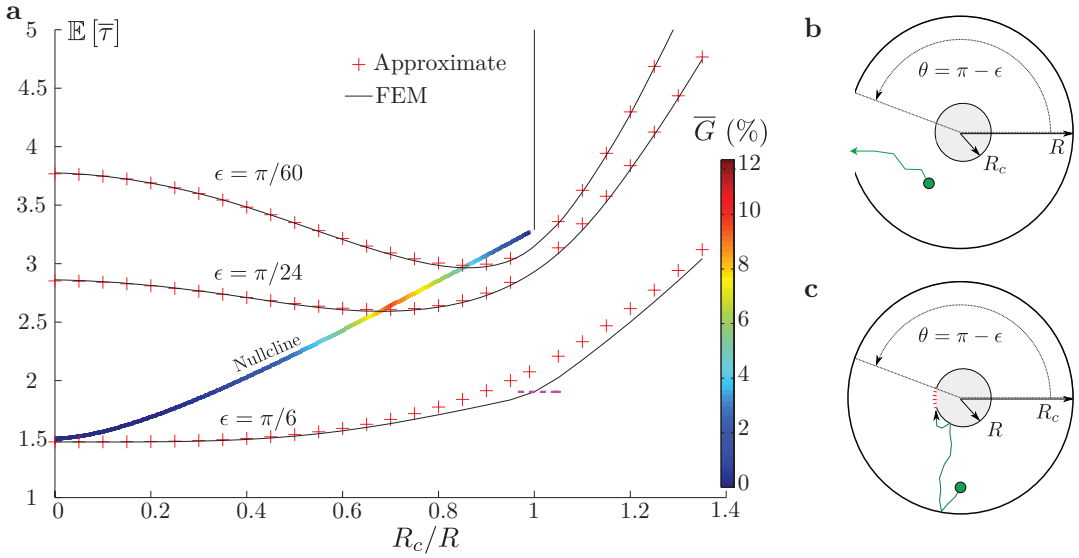

FIG. 8: (Color Online) **(a)** GMFPT to an exit of half-width ϵ for a Brownian particle confined in an annulus Ω of radii R_c and $R = 1$ (illustrated by **(b)** for $R_c > R$ and **(c)** for $R_c < R$). The approximate solution from Eq. (80) (red pluses) is compared to finite element method simulations (black solid line). The 1D GMFPT from Eq. (86), $(\pi - \epsilon)^3/(3\pi)$, is shown by magenta dotted line for $\epsilon = \pi/6$. The colored solid line indicates the loci of the minima of the GMFPT, with the color code being a function of the gain $\overline{G}$, defined by Eq. (90). The gain has a sharp maximum $G \approx 10\%$ for $R_c^{(c)} = 0.70$ and $\epsilon = 0.13 \ll 1$. (**b,c**) Two annuli with $R_c < 1$ (**b**) and $R_c > 1$ (**c**). The Brownian particle shown by green circle diffuses in the annulus before crossing the exit of half-width ϵ.

Eqs. (80) and (81) become

$$a_0^{(0)} \approx 2\frac{\pi^2}{3}, \tag{84}$$

$$a_n^{(0)} \approx \frac{2(-1)^{n-1}}{n^2}, \qquad n \geq 1, \tag{85}$$

hence the approximate expression for the MFPT (defined in Eq. (66)) is

$$\mathbb{E}\left[\tau_{(r,\theta)}\right] = \frac{1}{2}(\pi - \theta)(\pi + \theta) + \mathcal{O}(1 - R_c), \qquad \theta \in [0, \pi - \epsilon]\,. \tag{86}$$

The approximate expression is equal to the MFPT of a purely one-dimensional process up to $\mathcal{O}(\epsilon)$ terms. The average of Eq. (86) over all angles $\theta \in [0, \pi]$ is equal to $\pi^3/(3\pi)$, which is close to the exact result $(\pi - \epsilon)^3/(3\pi)$. Note that asymptotic formulas of Ref. [8] on the MFPT in 2D domains are not valid in the limit $R_c \to 1$.

(ii) In the large volume limit $R_c \gg 1$, we use Eq. (83) to show that the first Fourier coefficient of the MFPT reads

$$a_0^{(0)} \approx \left(R_c^2 - 1\right)\left(\alpha_0 + 4R_c^{-2}\right) + \mathcal{O}(1/R_c^4). \tag{87}$$

In the limit $\epsilon \ll 1$, the latter expansion can be identified with the result of Ref. [20] (p. 503) which is shown to be exact up to a $\mathcal{O}(\epsilon)$ term.

3. *Optimization of the GMFPT*

Now we focus on the GMFPT $\overline{\mathbb{E}[\tau]}$ defined in Eq. (13). In Fig. 8, we present the GMFPT as a function of R_c for different exit sizes ϵ. Interestingly, for small enough exit sizes $\epsilon < \epsilon_c$, the GMFPT is minimized for a specific value of the reflecting boundary radius $R_c^{(c)} < 1$.

In the narrow-escape limit $\epsilon \ll 1$, $R_c^{(c)} = 1$ is a global minimum of the GMFPT: the GMFPT at $R_c = 1$ converges to $\pi^2/3$ while the GMFPT diverges logarithmically with $\epsilon \ll 1$ for any other value

of $R_c \neq 1$. For increasing values of ϵ, the global minimum of the GMFPT is reached at smaller values $R_c^{(c)} < 1$. Eventually, the minimum $R_c^{(c)} = 0$ emerges for exit sizes larger than a threshold: $\epsilon_c \simeq 0.51$.

We determine an approximate value for the threshold ϵ_c based on the approximate expression (82) for the GMFPT. We first notice that for all $R_c \geq 1$, the GMFPT is a monotonically increasing function of R_c, hence $R_c^{(c)} \leq 1$. We define ϵ_c as the largest value of ϵ such that the GMFPT is a locally decreasing function at $R_c = 0$. This local condition is fulfilled if and only if the second derivative of the GMFPT $\overline{\mathbb{E}[\tau]}$ is negative at $R_c = 0$, leading to the following criterion on ϵ_c:

$$\alpha_0(\epsilon_c) = 4\alpha_1(\epsilon_c) - \frac{3}{4}, \tag{88}$$

where α_0 and α_1 are given in Eqs. (26a) and (26b). Assuming $\epsilon_c \ll 1$, Eq. (88) can be solved explicitly to get

$$\epsilon_c \approx \exp\left(\frac{8\ln(2) - 13}{16}\right) \approx 0.60, \tag{89}$$

In turn, the numerical solution of Eq. (88) yields $\epsilon_c \simeq 0.51$ which is close to the above estimate.

One may wonder how much time can be gained by setting R_c to the optimal $R_c^{(c)}$? We define the gain $\overline{G}$ as

$$\overline{G} = \frac{\min\left(\overline{\mathbb{E}[\tau]}_{R_c=0}\ ,\ \overline{\mathbb{E}[\tau]}_{R_c=1}\right) - \overline{\mathbb{E}[\tau]}_{R_c^{(c)}}}{\min\left(\overline{\mathbb{E}[\tau]}_{R_c=0}\ ,\ \overline{\mathbb{E}[\tau]}_{R_c=1}\right)}, \tag{90}$$

so that $\overline{G}$ lies between 0 and 1. The loci of the minima of the GMFPT are the set of points $(R_c^{(c)}, \overline{\mathbb{E}[\tau]}_{R_c^{(c)}})$ which are shown in Fig. 8 and colored according to the gain $\overline{G}$.

The gain has a sharp maximum $G \approx 10\%$ for $R_c^{(c)} \simeq 0.70$ and $\epsilon \simeq 0.13 \ll 1$. Notice that the optimal gain is obtained for a value of ϵ such that the GMFPT at $R_c = 0$ is approximately equal to the GMFPT at $R_c = 1$. The optimal $R_c^{(c)}$ results from a trade-off between two competing geometrical effects: (i) increasing $R_c \ll R$ reduces the accessibility to the exit for remote particles which have to circumvent the reflecting boundary at $r = R_c$; and (ii) once a particle is close to the exit, increasing R_c increases the probability for the particle to cross the exit.

B. Advection-diffusion with a radial bias

We consider a diffusive particle confined in a disk of radius R whose motion is biased by a $1/r$ velocity field $\vec{v}(r)$. The velocity field $\vec{v}(r)$ is characterized by a dimensionless parameter μ:

$$\vec{v}(r) = \frac{\mu D}{r^2}\,\vec{r}. \tag{91}$$

Note that $\mu > 0$ corresponds to an outward drift. Setting units by $R = 1$ and $D = 1$, the backward diffusion Eq. (14a) on the survival probability reads

$$\left(\Delta + \frac{\mu}{r}\partial_r\right)\ S^{(p)}(r,\theta) = p\ S^{(p)}(r,\theta) - 1, \qquad\qquad r \in [0,1), \quad \theta \in [0, 2\pi). \tag{92}$$

A separation of variables method provides the set $f_n^{(p)}\cos(n\theta)$ of solutions for Eq. (92), see Table II.

The approximate scheme of Sec. II B 3 leads to an explicit expression for the MFPT. We substitute $\mathcal{C}^{(0)}$ by $\mathcal{C}_a^{(0)}$ (defined in Eq. (55)) into Eqs. (52a) and (52b) and use the expressions of Table II to get the following approximation for the Fourier coefficients of the MFPT:

$$a_0^{(0)} \approx \frac{2}{2+\mu}\left\{\alpha_0 + \sum_{k=1}^{\infty} 2k\left[-1 + \frac{\mu}{2k} + \sqrt{1 + \left(\frac{\mu}{2k}\right)^2}\right]\alpha_k^2\right\}, \tag{93}$$

$$a_n^{(0)} \approx \frac{2}{2+\mu}\ \frac{\alpha_n}{\sqrt{1 + \left(\frac{\mu}{2n}\right)^2} - \frac{\mu}{2n}}, \qquad n \geq 1. \tag{94}$$

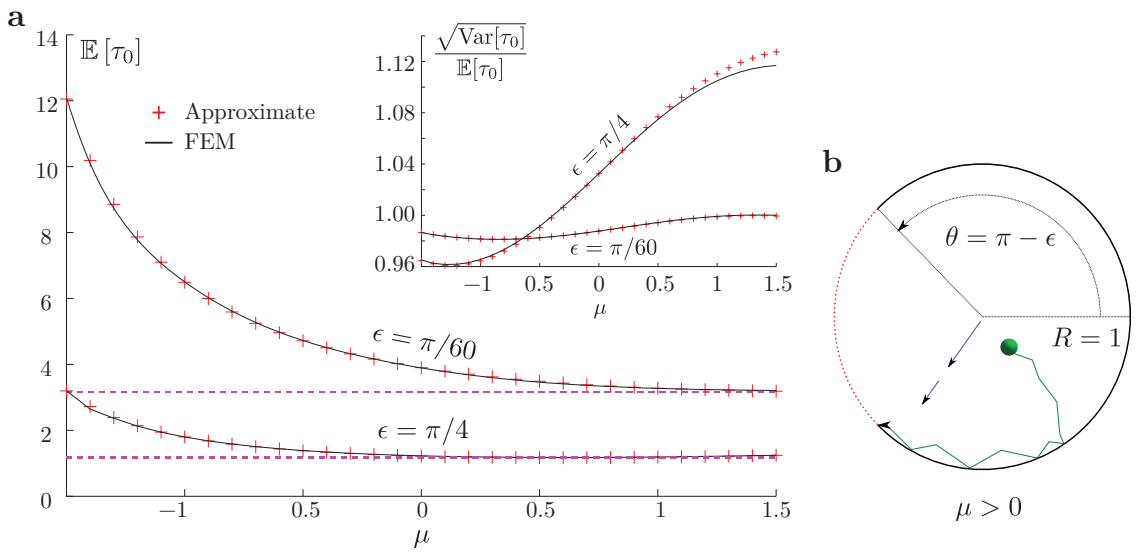

FIG. 9: (Color Online) (**a**) The MFPT $\mathbb{E}[\tau_0]$ to an exit of half-width $\epsilon = \pi/4$ for Brownian particles whose diffusive motion is biased by a $1/r$ velocity field $\vec{v}(r) = \mu D\vec{r}/r^2$. Particles are started at $r = 0$ inside the unit disk [as sketched in (**b**)]. The analytical approximation in Eq. (93) (red pluses) is compared to a finite element method (denoted FEM, black solid line). The 1D GMFPT from Eq. (86), i.e., $(\pi - \epsilon)^3/(3\pi)$, is shown by horizontal magenta dashed lines. The ratio of the standard deviation to the MFPT is represented in the inset. Note that the smaller the ϵ, the closer this ratio is to 1. **(b)** A Brownian particle (shown by green circle) is advected by a radial flow field $\vec{v}(r) = \mu D\,\vec{r}/r^2$, with $\mu > 0$ corresponding to an outward drift (blue arrows). The particle is reflected by the boundary at $r = 1$ before crossing the exit (shown by red dashed line) of half width $\epsilon = \pi/4$.

where α_n are defined by Eqs. (27b). The MFPT can be computed from Eq. (66). The GMFPT, defined in Eq. (13), is

$$\overline{\mathbb{E}[\tau]} \approx \frac{1}{2+\mu}\left\{\alpha_0 + \sum_{k=1}^{\infty} 2k\left[-1 + \frac{\mu}{2k} + \sqrt{1+\left(\frac{\mu}{2k}\right)^2}\right]\alpha_k^2\right\} + \frac{1}{4(2+\mu)}. \tag{95}$$

In Fig. 9, we compare the approximate MFPT $\mathbb{E}[\tau_0]$ (for a particle started at $r = 0$) to the result obtained by a finite element method. The MFPT diverges for all $\mu \leq -2$: the inward drift strongly confines particles at $r = 0$. In the limit $\mu \gg 1$, the MFPT converges to the MFPT of a 1D process given by Eq. (86), up to a small $\mathcal{O}(\epsilon)$ correction. The MFPT is a monotonically decreasing functions of μ, as illustrated in Fig. 9(a), and there is no optimal drift which minimizes the MFPT.

C. Rectangles

We consider the confining domain Ω to be a rectangle $\Omega = [0, R] \times [0, \phi]$ with reflecting edges at $r = 0$, $\theta = 0$ and $\theta = \phi$. The boundary at $r = R$ is reflecting except for an absorbing segment of length ϵ at the corner, as illustrated in Fig. 10(b). Setting units by $\phi = \pi$ and $D = 1$, the Helmholtz equation on the survival probability reads [1, 27]

$$\left(\frac{\partial^2}{\partial r^2} + \frac{\partial^2}{\partial \theta^2}\right) S^{(p)}(r,\theta) = p\; S^{(p)}(r,\theta) - 1 \qquad (r,\theta) \in \Omega. \tag{96}$$

Although our approach allows one to get the whole FPT distribution, we focus on obtaining an explicit expression for the MFPT. We substitute $\mathcal{C}^{(0)}$ by $\mathcal{C}_a^{(0)}$ (defined in Eq. (55)) in Eqs. (52a) and (52b) and use the expressions of Table II to get the following approximation for the Fourier coefficients of the

MFPT:

$$a_0^{(0)} \approx 2R\left\{\alpha_0 + \sum_{k=1}^{\infty}\left[-1+\coth(kR)\right]4k\alpha_k^2\right\}, \tag{97}$$

$$a_n^{(0)} \approx \frac{2R}{\coth(nR)}\alpha_n, \qquad n \geq 1, \tag{98}$$

where α_n are defined Eqs. (27b). Using Eq. (97) and (98), the MFPT can be computed from Eq. (66). Figure 10 shows the approximate MFPT as a function of the initial position $(r,\theta) \in \Omega$ for $R = 1$ and $\phi = \pi$. We also compute the standard deviation, skewness, and excess kurtosis through the approximate resolution scheme of Eqs. (97) and (98). The error of the approximate solution to the numerical and exact resolution scheme is below 2% (the error is maximal close to the edges of the exit).

The GMFPT, defined in Eq. (13), is

$$\overline{\mathbb{E}\left[\tau\right]} \approx R\left\{\alpha_0 + \sum_{k=1}^{\infty}\left[-1+\coth(kR)\right]4k\alpha_k^2\right\} + \frac{R^2}{3}. \tag{99}$$

In the limit $R \ll \phi = \pi$, the GMFPT converges to the GMFPT of a 1D process given by Eq. (86), up to small $\mathcal{O}(\epsilon)$ correction. In the opposite limit $R \gg 1$, the relation

$$-1+\coth(kR) = -1 + \frac{1+\exp(-2kR)}{1-\exp(-2kR)} = 2\beta^2 + \mathcal{O}(\beta^4) \tag{100}$$

with $\beta = \exp\left(-R\right)$, leads to

$$a_0^{(0)} \approx 4R\left[\ln\left(\frac{2}{\epsilon}\right) + 2\beta^2\right] + \mathcal{O}(\beta^4) \tag{101}$$

in the small $\epsilon \ll 1$ limit. The latter expression can be identified with the result presented in [20] (p. 496), which is shown to be exact up to a $\mathcal{O}(\epsilon)$ term.

D. Analogy to heat transfer problems

We show that the resolution scheme of Sec. II B provides the evolution of temperature in a room Ω with adiabatic walls which include a centered window of width 2ϵ. In fact, the evolution of temperature $\tilde{T}^{(t)}(r,\theta)$ is governed by the heat equation [22, 23]

$$\frac{\partial \tilde{T}^{(t)}(r,\theta)}{\partial t} = D\Delta\tilde{T}^{(t)}(r,\theta). \tag{102}$$

The temperature in the room Ω is supposed to be homogeneous before opening the window at time $t = 0$: $\tilde{T}^{(0)}(r,\theta) = T_1$. Since that moment and for all $t > 0$, the boundary condition at the window is $\tilde{T}^{(t)}(r,\theta) = T_0$, where T_0 is an exterior temperature. Along the adiabatic walls the temperature $\tilde{T}^{(t)}(r,\theta)$ satisfies the reflecting boundary condition. The function

$$\tilde{w}^{(t)}(r,\theta) = \frac{\tilde{T}^{(t)}(r,\theta) - T_0}{T_1 - T_0}. \tag{103}$$

satisfies (i) the heat Eq. (102), (ii) Dirichlet boundary condition at the window ($\tilde{w}^{(t)}(r,\theta) = 0$ for all $t > 0$), (iii) Neumann boundary condition along the adiabatic walls, and (iv) the initial condition $\tilde{w}^{(0)}(r,\theta) = 1$. Since the survival probability satisfies the same equations, one concludes that $\tilde{w}^{(t)}(r,\theta) = \tilde{S}^{(t)}(r,\theta)$.

E. Analogy to microchannel flows

Large pressure drops are necessary to cause liquid flow in microchannels due to viscous dissipation at the boundary (no-slip condition). In order to increase the flow rate (at a given pressure drop), one

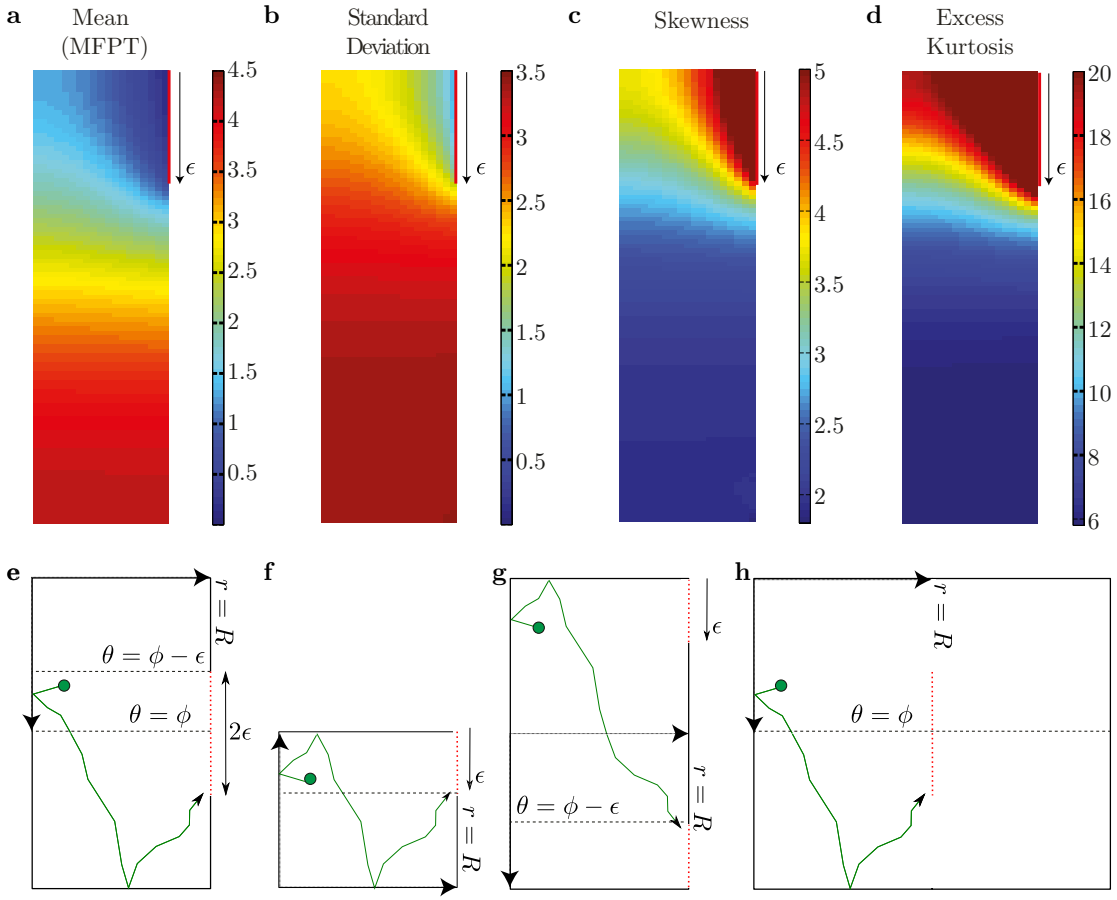

FIG. 10: (Color Online) **Upper panel**: The cumulants of the exit time as functions of the starting position of the Brownian particle within the rectangle $\Omega = [0, R] \times [0, \phi]$ with $R = 1$ and $\phi = \pi$. The exit (shown by red line and an arrow) is a linear segment of total width $\epsilon = \pi/4$ on the edge of length π. The cumulants computed through the approximate resolution of Eqs. (97) and (98): (**a**) MFPT; (**b**) standard deviation; (**c**) skewness; and (**d**) excess kurtosis. **Lower panel**: The distribution of the FPT is identical for the four cases: (**e**) rectangle $\Omega = [0, R] \times [0, 2\phi]$ with reflecting walls, pierced by a centered opening of width 2ϵ; (**f**) rectangle $\Omega = [0, R] \times [0, \phi]$ with reflecting walls, pierced by an opening of width ϵ located in a corner; (**g**) rectangle $\Omega = [0, R] \times [0, 2\phi]$ with reflecting walls, pierced by two cornered openings, each of width ϵ; and (**h**) rectangle $\Omega = [0, 2R] \times [0, 2\phi]$ with reflecting walls and a centered linear absorbing region (vertical red dashed line) of total width 2ϵ. Green circle represents the position of a particle in these rectangles.

can introduce ultra-hydrophobic grooves so that the layer of gas trapped within the grooves would act as an air-cushion for the fluid flow [25, 26]. We consider an array of ultra-hydrophobic grooves aligned in the direction of the pressure drop z obtained by a periodic repetition of a fundamental cell of width $\theta = 2\phi$. The floor of the microchannel is at the depth $r = R$ (see Fig. 11). The top surface at $r = 0$ can be assumed to be either (i) a free surface such that the shear stress is equal to zero, or (ii) a no-slip surface (as considered in Ref. [24]).

In the case of a no-slip condition at $r = R$ (case (ii)) and in the limit $R \gg \phi$, an exact solution of the stationary flow was found in terms of the set (α_n) defined in Eqs. (26a) and (26b) [24]. In this section we show how our method can be adapted to provide: (i) an approximate solution for the flow which is accurate for any value of R, and (ii) an exact resolution scheme as well as an approximate explicit expression for a time-dependent problem, i.e., the evolution of the flow from a given radial profile at $t = 0$ to the steady state profile at $t = \infty$.

The flow is assumed to be (i) Newtonian and incompressible, (ii) at zero Reynolds number, (iii) in the absence of external force (e.g. gravitational force), and (iv) under a constant pressure gradient $\frac{\partial p}{\partial z} = q$.

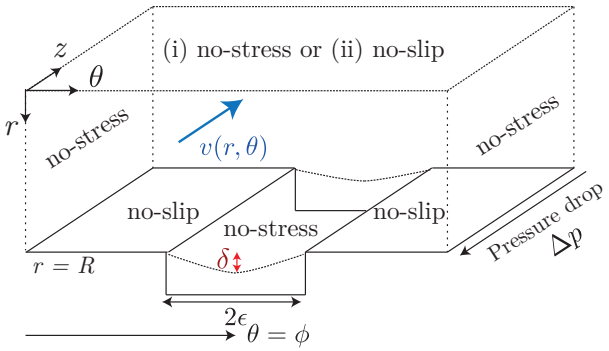

FIG. 11: (Color Online) Scheme of the microchannel flow problem, in which the floor of a channel of depth R contains a large number of regularly spaced grooves of width 2ϵ parallel to the flow direction ($0z$). This structure can be modeled by the periodic repetition of a fundamental cell of width 2ϕ, resulting in a no-shear condition $\theta = 0$ and $\theta = 2\phi$. The shear stress is assumed to be zero along the free surfaces within the groove at $r = R$ (the free surface lies above trapped gas phase). In turn, non-slip boundary condition is imposed on the remaining part of the groove. The top surface at $r = 0$ can be assumed to be: (i) a free surface along which the shear stress is assumed to be zero (ii) a no-slip surface (i.e. the case considered in Ref. [24]). The problem consists in determining the stationary velocity profile $v^{(\infty)}(r, \theta)$ for an incompressible Newtonian fluid at low Reynolds numbers and under constant pressure drop.

Under these assumptions the Navier-Stokes equation on the velocity profile $\tilde{v}^{(t)}(r, \theta)$ reads as

$$\rho \frac{\partial \tilde{v}^{(t)}(r,\theta)}{\partial t} = \mu \Delta \tilde{v}^{(t)}(r,\theta) + q, \qquad (r,\theta) \in [0,\, R] \times [0, 2\phi], \tag{104}$$

where ρ is the mass density of the fluid and μ its viscosity. In dimensionless variables $\theta \leftarrow \pi\theta/\phi$, $R \leftarrow \pi R/\phi$, $\tilde{v}^{(t)} \leftarrow (\pi/\phi)^2(\mu/q)\tilde{v}^{(t)}$ and $t \leftarrow (\mu\phi^2 t)/(\rho\pi^2)$, Eq. (104) becomes

$$\frac{\partial \tilde{v}^{(t)}(r,\theta)}{\partial t} = \Delta \tilde{v}^{(t)}(r,\theta) + 1, \qquad (r,\theta) \in [0,\, R] \times [0,\, 2\pi] \tag{105}$$

In the stationary regime ($t = \infty$), Eq. (105) reads

$$\Delta \tilde{v}^{(\infty)}(r,\theta) = -1, \qquad (r,\theta) \in [0,\, R] \times [0,\, 2\pi]. \tag{106}$$

The latter equation on the stationary flow $\tilde{v}^{(\infty)}(r, \theta)$ can be identified with the equation on the MFPT (e.g. Eq. (14a) at $p = 0$). The Laplace transform of Eq. (105) is

$$\Delta\, v^{(p)}(r,\theta) = p\; v^{(p)}(r,\theta) - \tilde{v}^{(0)}(r) - \frac{1}{p}, \tag{107}$$

where $\tilde{v}^{(0)}(r)$ is the initial velocity profile at $t = 0$, which is assumed to be independent of θ. Note that the long-time flow profile $\tilde{v}^{(\infty)}(r, \theta)$ can be deduced from $v^{(p)}(r, \theta)$ through the relation:

$$\lim_{p\to 0}\; p\, v^{(p)}(r,\theta) = \tilde{v}^{(\infty)}(r,\theta). \tag{108}$$

Eq. (107) is completed by the following boundary conditions. The shear stress is assumed to be zero along the free surfaces, i.e., at $\theta = 0$, $\theta = 2\pi$, $r = 0$, and within the groove at $r = R$ (the free surface lies above the gas trapped within the groove). We consider the case $\delta = 0$, where δ is the maximum penetration of the free surface into the groove. This approximation is justified because the surface of the groove is hydrophobic. At the bottom surface $r = R$, the velocity field satisfies the mixed boundary conditions:

- non-slip conditions along the hydrophobic surface: $v^{(p)}(r, \theta) = 0$ for all $\theta \in [\pi - \epsilon, \pi + \epsilon]$ (similar to Eq. (18b)),
- no-shear conditions along the free surface: $\left[\partial_r v^{(p)}(r,\theta)\right]_{r=R} = 0$ for all $\theta \in [0, \pi - \epsilon) \cup (\pi + \epsilon, 2\pi]$ (similar to Eq. (18c)).

Similarly to Eq. (16), we define the auxiliary function

$$u^{(p)}(r,\theta) \equiv v^{(p)}(r,\theta) - v_\pi^{(p)}(r), \tag{109}$$

where $v_\pi^{(p)}(r)$ is the rotation invariant solution of Eq. (107) satisfying $v_\pi^{(p)}(1) = 0$, and either $\partial_r S_\pi^{(p)}(r) = 0$ at $r = 0$ for a free surface (i), or $v_\pi^{(p)}(1) = 0$ at $r = 0$ for a no-slip surface (ii).

The Fourier expansion of the function $u^{(p)}(r,\theta)$ according to Eq. (19) defines the Fourier coefficients $a_n^{(p)}$. In the case of free surface, functions $f_n^{(p)}$ are given in Table II. In the case of a no-slip surface, functions $f_n^{(p)}$ read

$$f_n^{(p)}(r) = \frac{\sinh(\sqrt{p+n^2}\ r)}{\sinh(\sqrt{p+n^2}R)}, \qquad n \geq 0. \tag{110}$$

The Fourier coefficients $a_n^{(p)}$ are shown to satisfy Eqs. (33a) and (33b). One can therefore apply the resolution scheme presented in Sec. II B to derive both an exact and an approximate expression for the Laplace transform $v^{(p)}(r,\theta)$ of the flow velocity. An approximate expression for stationary velocity profile $\tilde{v}^{(\infty)}(r,\theta)$ is then deduced from Eq. (108).

Conclusion

We studied the Helmholtz equation with mixed boundary conditions on spherically symmetric two-dimensional domains (disks, angular sectors, annuli). This classical boundary value problem describes how diffusive particles exit from a domain through an opening on the reflecting boundary. The Dirichlet boundary condition on the opening is mixed with Neumann boundary condition on the remaining part of the boundary that presents the major challenge in the resolution of this problem. For this reason, most previous studies were focused on the asymptotic analysis for small exits. In order to overcome this limitation, we developed a new approach, in which the problem is reduced to a set of linear equations on the Fourier coefficients of the survival probability. We provide then two resolution schemes which are applicable for arbitrary exit size. The first scheme is exact but it relies on a numerical solution of linear equations and requires thus a matrix inversion. In turn, the second scheme is explicit (without matrix inversion) but approximate. As a result, we managed to derive the whole distribution of first passage times and their moments for the escape problem with arbitrary exit size. The approximate solution was shown to be accurate over the whole range of times. Both analytical solutions have been successfully verified by extensive numerical simulations, through both a finite element method resolution of the original boundary value problem, and by Monte Carlo simulations.

Using this method, we analyzed the behavior of the FPT probability density for various initial positions. When the initial position is far from the exit, the FPT probability density was shown to be accurately approximated by an exponential distribution. In this situation, the whole distribution of FPTs is essentially determined by the MFPT for which we derived exact explicit relations.

The developed method is also applied to rectangular domains and to biased diffusion with a radial drift within a disk. Since the Helmholtz equation with mixed boundary conditions is also encountered in microfluidics [24], heat propagation [22, 23], quantum billiards [35, 36], and acoustics [37], the developed method can find numerous applications beyond first passage processes.

Acknowledgments

O.B. is supported by the ERC Starting Grant No. FPTOpt-277998. D.G. is supported by an ANR project “INADILIC”.

The final publication is available at Springer via:

http://link.springer.com/article/10.1007%2Fs10955-014-1116-6.

Appendix A: Simplification of α_n and M_{nm}

1. Simplified expressions for α_0

Herewith we prove the following identity for all $0 \leq t < \pi$

$$\frac{\sqrt{2}}{\pi}\int_0^t \mathrm{d}x \frac{x\sin(x/2)}{\sqrt{\cos x - \cos t}} = -2\ln\left(\cos\left(\frac{t}{2}\right)\right). \tag{A1}$$

We proceed by a change of variable $z = \cos x$ in the left-hand side term of Eq. (A1) and we denote $T = \cos(t)$:

$$\int_0^t \mathrm{d}x \frac{x\sin(x/2)}{\sqrt{\cos x - \cos t}} = \int_T^1 \mathrm{d}z \left[\frac{\arccos z}{\sqrt{2\,(1+z)}}\right]\frac{1}{\sqrt{z-T}}. \tag{A2}$$

We write the right-hand side of Eq. (A1) in the form

$$-2\log\left(\cos\left(\frac{t}{2}\right)\right) = \log\left(\frac{2}{1+T}\right). \tag{A3}$$

From Ref. [15], the Abel's equation

$$\int_T^1 \frac{y(z)\mathrm{d}z}{\sqrt{z-T}} = \frac{\pi}{\sqrt{2}}\log\left(\frac{2}{1+T}\right) \tag{A4}$$

has an unique solution for all $-1 < X < 1$

$$y(z) = \frac{1}{\pi}\frac{\pi}{\sqrt{2}}\int_1^z \frac{\mathrm{d}u}{\sqrt{u-z}(1+z)} = \frac{\arccos z}{\sqrt{2(1+z)}}. \tag{A5}$$

Identification of the kernels of Eqs. (A2) and (A5) proves the identity (A1).

The expression for α_0 from Eq. (27a) is found by setting $t = \pi - \epsilon$ in Eq. (A2). Note that the obtained expression for α_0 from Eq. (27a) could also be deduced from the expression of the MFPT from Ref. [16].

2. Simplified expressions for $\alpha_n, n \geq 1$

The solution of Eqs. (24a), (24b) is given in [8] in the form:

$$\alpha_n = \frac{1}{\sqrt{2}\pi}\int_0^{\pi-\epsilon}\mathrm{d}t\left(\frac{\partial}{\partial t}\int_0^t \mathrm{d}x\frac{x\sin(x/2)}{\sqrt{\cos x - \cos t}}\right)\big[P_n(\cos t) + P_{n-1}(\cos t)\big], \qquad n \geq 1. \tag{A6}$$

Using the identity (A1), we show that

$$\alpha_n = \frac{1}{2}\int_0^{\pi-\epsilon}\mathrm{d}t\tan\left(\frac{t}{2}\right)\big[P_n(\cos t) + P_{n-1}(\cos t)\big], \qquad n \geq 1. \tag{A7}$$

After the change of variable $u = \cos t$, the latter identity leads to

$$\alpha_n = \frac{1}{2}\int_{-\cos\epsilon}^1 \frac{\mathrm{d}u}{1+u}\big[P_n(u) + P_{n-1}(u)\big], \qquad n \geq 1. \tag{A8}$$

We now use the identity

$$\frac{\partial}{\partial x}\left(\frac{P_m(x) - P_{m-1}(x)}{m}\right)_{|x=X} = \frac{P_m(X) + P_{m-1}(X)}{1+X}, \qquad m \geq 1, \tag{A9}$$

which is valid for all $X \in [-1, 1]$, to obtain the announced result:

$$\alpha_n = \frac{(-1)^{n-1}}{2n}\big[P_n(\cos\epsilon) + P_{n-1}(\cos\epsilon)\big], \qquad n \geq 1. \tag{A10}$$

3. Simplified expression for M_{nm}

The expression for M_{nm} from Eq. (46) can be simplified using Mehler's integral representation (35):

$$M_{nm} = \frac{1}{2}\int_0^{\pi-\epsilon} \mathrm{d}t \left\{ \frac{\partial}{\partial t}\left[P_m(\cos t) - P_{m-1}(\cos t)\right]\right\}\left[P_n(\cos t) + P_{n-1}(\cos t)\right], \qquad n \geq 1, \quad m \geq 1. \tag{A11}$$

The identity Eq. (A9) then leads to the announced expression (47). Notice that the following matrix

$$S_{nm} = \sqrt{\frac{n}{m}} M_{nm}, \qquad n \geq 1, \quad m \geq 1, \tag{A12}$$

is symmetric. The eigenvalues of S_{nm} are real, and so are the eigenvalues of M. In Sec. A 5 we show that the coefficients α_n are given by an eigenvector of the infinite-dimensional matrix M.

4. Perturbative expansion of M_{nm}

We first derive an alternative identity to Eq. (A9). Let us define

$$A_n(x) \equiv \frac{\partial}{\partial x}(P_n(x) - P_{n-1}(x)), \qquad n \geq 1. \tag{A13}$$

Using the recurrence formulas for Legendre polynomials, we obtain

$$A_n(x) = (P_n'(x) - P_{n-2}'(x)) - (P_{n-1}'(x) - P_{n-2}'(x)) = (2n-1)P_{n-1}(x) - A_{n-1}(x) = \sum_{k=1}^{n}(-1)^{n-k}(2k-1)P_{k-1}(x), \tag{A14}$$

where we used $P_0(x) = 1$, $P_1(x) = x$, and $A_1(x) = 1 = (2-1)P_0(x)$.

Combining Eq. (A11) and the identity (A14) we obtain the announced result:

$$\begin{aligned} M_{nm} &= \int_0^{\pi-\epsilon} \mathrm{d}t\ \frac{\sin t}{2} A_m(\cos t)\left[P_n(\cos t) + P_{n-1}(\cos t)\right], \\ &= \sum_{k=1}^{m}(-1)^{n-k}(2k-1)\left(K_{k-1,n-1} + K_{k-1,n}\right), \end{aligned} \tag{A15}$$

where the coefficients $K_{k,n}$ are defined by

$$K_{k,n} \equiv \int_0^{\pi-\epsilon} \mathrm{d}t\ P_k(\cos t)P_n(\cos t)\frac{\sin t}{2}. \tag{A16}$$

In the leading order in $\epsilon \ll 1$, Eq. (A15) reads

$$M_{nm} = \sum_{k=1}^{m}(-1)^{n-k}(2k-1)\left(\frac{\delta_{k-1,n-1}}{2n-1} + \frac{\delta_{k-1,n}}{2n+1}\right) + \mathcal{O}(\epsilon). \tag{A17}$$

If $m < n$, it is straightforward to show that $M_{nm} = \mathcal{O}(\epsilon)$. If $m > n$, $M_{nm} = \mathcal{O}(\epsilon)$ as successive terms with $k = n$ and $k = n+1$ cancel each other. The matrix M_{nm} $(n, m \geq 1)$ is thus diagonal at the first order in ϵ:

$$M_{nm} = \delta_{nm} + \mathcal{O}(\epsilon). \tag{A18}$$

In order to get the next term in the series expansion in $\epsilon \ll 1$, we write

$$M_{nm} - \delta_{nm} = -\frac{m}{2}\int_{-1}^{-\cos\epsilon} \frac{1}{1+x}\left[P_m(x) + P_{m-1}(x)\right]\left[P_n(x) + P_{n-1}(x)\right]\mathrm{d}x, \qquad n \geq 1, \quad m \geq 1. \tag{A19}$$

We now focus on the term in the right-hand side of Eq. (A19). In the vicinity of $x = -1$, the integrand of Eq. (A19) expands into

$$\frac{1}{1+x}\big[P_m(x)+P_{m-1}(x)\big]\big[P_n(x)+P_{n-1}(x)\big] = \frac{nm(-1)^{n+m}}{8}(1+x)+\mathcal{O}(1+x). \tag{A20}$$

Notice that

$$\int_{-1}^{-\cos\epsilon}(1+x)\mathrm{d}x = \frac{\epsilon^4}{8}+\mathcal{O}(\epsilon^5). \tag{A21}$$

Substituting Eqs. (A20) and (A21) into Eq. (A19) leads to

$$M_{nm} = \delta_{mn}+\frac{nm^2(-1)^{n+m}}{8}\epsilon^4+\mathcal{O}(\epsilon^5). \tag{A22}$$

5. Summation identities

Using the identities for sums of Legendre polynomials from Ref. [38], we derive the following equation

$$S \equiv \sum_{m=1}^{\infty}(-1)^{m-1}\big[P_m(\cos x)+P_{m-1}(\cos x)\big]\big[P_m(\cos\epsilon)+P_{m-1}(\cos\epsilon)\big] = 2, \qquad 0<x<\pi-\epsilon. \tag{A23}$$

To prove this identity, we first use the Mehler's representation (35) for Legendre polynomials $P_m(\cos\epsilon)$ and $P_{m-1}(\cos\epsilon)$ to obtain

$$S = \frac{2}{\pi}\int_0^{\pi-\epsilon}\frac{\sum_{m=1}^{\infty}\big[P_m(\cos x)+P_{m-1}(\cos x)\big]\,\big[\cos(\big(m+\frac{1}{2}\big)\,t)-\cos(\big(m-\frac{1}{2}\big)\,t)\big]}{\sqrt{(\cos(t)+\cos\epsilon)(\cos x-\cos(t))}}, \qquad 0<x<\pi. \tag{A24}$$

We then use trigonometric identities and the series identity (39) to obtain the following integral representation

$$S = -\frac{2}{\pi}\int_x^{\pi-\epsilon}\mathrm{d}t\frac{2\sin\left(\frac{t}{2}\right)\cos\left(\frac{t}{2}\right)}{\sqrt{(\cos(t)+\cos\epsilon)(\cos x-\cos(t))}}, \qquad 0<x<\pi-\epsilon. \tag{A25}$$

The consecutive change of variables $z = \cos(t)$ and $U = \sqrt{(z+\cos\epsilon)(\cos x - z)}$ leads to

$$S = \frac{2}{\pi}\int_{-\cos x}^{\cos x}\frac{\mathrm{d}z}{\sqrt{(z+\cos\epsilon)(\cos x-z)}} = 2, \tag{A26}$$

which proves the identity (A23). We will use this identity in the following form:

$$\sum_{m=1}^{\infty}\big[P_m(\cos x)+P_{m-1}(\cos x)\big]m\ \alpha_m = 1, \qquad 0<x<\pi-\epsilon. \tag{A27}$$

where α_m are given by Eq. (27b).

a. *Proof of the identity (83)*

We write α_m from Eq. (25b) and exchange the sum and the integral to obtain:

$$\sum_{m=1}^{\infty}2m\alpha_m^2 = \frac{\sqrt{2}}{\pi}\int_0^{\pi-\epsilon}\mathrm{d}t\left(\frac{\partial}{\partial t}\int_0^t\mathrm{d}x\frac{x\sin(x/2)}{\sqrt{\cos x-\cos t}}\right)\left(\sum_{m=1}^{\infty}\big[P_m(\cos t)+P_{m-1}(\cos t)\big]m\alpha_m\right). \tag{A28}$$

Using the identity (A23) in the right-hand side of Eq. (A28) and the representation (25a) of α_0 leads to the result of Eq. (83).

b. An eigenvector of the matrix M

We show that the coefficients α_n (with $n \geq 1$) form an eigenvector of the matrix M:

$$\sum_{m=1}^{\infty} M_{nm}\alpha_m = \alpha_n. \tag{A29}$$

We express M_{nm} through Eq. (47) and exchange the sum and the integral:

$$\sum_{m=1}^{\infty} M_{nm}\alpha_m = \frac{1}{2}\int_{-\cos(\epsilon)}^{1} \frac{1}{1+x}\left(P_n(x)+P_{n-1}(x)\right)\left(\sum_{m=1}^{\infty}\left[P_m(\cos t)+P_{m-1}(\cos t)\right]m\alpha_m\right)\mathrm{d}x, \tag{A30}$$

from which the identity (A23) leads to the announced identity (A29).

Appendix B: Spatially averaged variances

We denote by $\overline{\mathbb{E}\left[\tau^n\right]}$ the spatial average of the n-th moment of the exit time:

$$\overline{\mathbb{E}\left[\tau^n\right]} \equiv \frac{1}{\pi}\int_{\vec{r}_0\in\Omega} \mathrm{d}\vec{r}_0\ \mathbb{E}\left[\tau_{\vec{r}_0}^n\right], \tag{B1}$$

where $\mathrm{d}\vec{r}_0$ is the uniform measure over Ω. Let us now consider the random variable τ_Ω, defined in Sec. II D 1 as the exit time of a particle started at a random starting position X. The n-th moment τ_Ω reads

$$\mathbb{E}\left[\tau_\Omega^n\right] \equiv \int_{\vec{r}_0\in\Omega} \mathrm{d}\mu(X=\vec{r}_0)\mathbb{E}\left[\tau_X^n\right], \tag{B2}$$

where $\mathrm{d}\mu(X=\vec{r}_0)$ is the probability density for X to be started at the position $\vec{r}_0$. If $\mathrm{d}\mu(X=\vec{r}_0)=\mathrm{d}\vec{r}_0$ is the uniform probability distribution, we can identify Eqs. (B1) and (B2), $\mathbb{E}\left[\tau_\Omega^n\right]=\overline{\mathbb{E}\left[\tau^n\right]}$, and the variance of the random variable τ_Ω is

$$\mathrm{Var}\left[\tau_\Omega\right] \equiv \left(\int_{\vec{r}_0\in\Omega} \mathrm{d}\mu(X=\vec{r}_0)\mathbb{E}\left[\tau_X^2\right]\right) - \left(\int_{\vec{r}_0\in\Omega} \mathrm{d}\mu(X=\vec{r}_0)\mathbb{E}\left[\tau_X\right]\right)^2 = \overline{\mathbb{E}\left[\tau^2\right]} - \overline{\mathbb{E}\left[\tau\right]}^2. \tag{B3}$$

Note that $\mathrm{Var}\left[\tau_\Omega\right]$ differs from the spatial average of the variance: $\mathrm{Var}\left[\tau_\Omega\right] \neq \overline{\mathrm{Var}\ \tau} = \overline{\mathbb{E}\left[\tau^2\right]} - \overline{\mathbb{E}\left[\tau\right]^2}$, because $\overline{\mathbb{E}\left[\tau\right]}^2 \neq \overline{\mathbb{E}\left[\tau\right]}^2$.

Appendix C: Convergence to an exponential distribution in the narrow-escape limit

1. From the expression for the survival distribution

We recall that the expressions for $(\alpha_n), n \geq 0$, in the limit $\epsilon \ll 1$ are provided in Eqs. (59a)–(59b). We denote by $\tilde{S}_e(t)$ the normalized single exponential distribution whose mean is equal to the GMFPT defined in Eq. (13). The Laplace transform of the distribution $\tilde{S}_e^{(t)}$ is

$$S_e^{(p)} = \frac{\overline{\mathbb{E}\left[\tau\right]}}{1+p\ \overline{\mathbb{E}\left[\tau\right]}}. \tag{C1}$$

We show that in the narrow-escape limit ($\epsilon \ll 1$), the averaged exit time distribution $\overline{S^{(p)}} \approx a_0^{(p)}/2$ converges to $S_e^{(p)}$, as expected from Ref. [12]. Due to the divergence of the coefficient α_0 from Eq. (59a), the asymptotic expansion of Eq. (52a) at the first order in $\epsilon \ll 1$ reads

$$\frac{a_0^{(p)}}{2} = \alpha_0\left[\partial_r f_0^{[1]}\right]_{|r=1}\left[\sum_{k=0}^{\infty}\left(p\left[\partial_r f_0^{[1]}\right]_{|r=1}\alpha_0\right)^k\right] + \mathcal{O}(\epsilon). \tag{C2}$$

where $\left[\partial_r f_0^{[1]}\right]_{|r=1}$ is the first-order expansion in $p \ll 1$ of $\left[\partial_r f_0^{(p)}\right]_{|r=1}$. At the leading order in ϵ, the averaged survival probability over Ω is

$$\overline{S^{(p)}} = \frac{\alpha_0 \left[\partial_r f_0^{[1]}\right]_{|r=1}}{1 + \alpha_0 \left[\partial_r f_0^{[1]}\right]_{|r=1}} + \mathcal{O}(\epsilon). \tag{C3}$$

Combining Eqs. (21) and (52a), the GMFPT at the leading order in $\epsilon \ll 1$ is

$$\overline{\mathbb{E}\left[\tau\right]} = \alpha_0 \left[\partial_r f_0^{[1]}\right]_{|r=1} + \mathcal{O}(\epsilon). \tag{C4}$$

Combining Eqs. (C1) and (C3) leads to

$$\overline{S^{(p)}} = \overline{S_e^{(p)}} + \mathcal{O}(\epsilon). \tag{C5}$$

This shows the convergence in law of the FPT distribution to an exponential distribution whose mean is the GMFPT as expected for the narrow-espace limit [12].

2. From the expression for the moments

Let us consider the random variable τ_Ω, defined in Sec. II D 1 as the exit time of a particle started at a random starting position. We provide a positive answer to the following question: does the distribution of τ_Ω converge to an exponential distribution in the limit $\epsilon \ll 1$, even though the starting positions within the boundary layer contribute to the statistics of τ_Ω? Using the recurrence scheme of Sec. II D 1, we verify that at the leading order in $\epsilon \ll 1$ the moments of τ_Ω are

$$\mathbb{E}\left[\tau_\Omega^n\right] = n! \left(\frac{\alpha_0}{2}\right)^n + \mathcal{O}(\ln(\epsilon)^{n-1}), \tag{C6}$$

which leads to $\mathbb{E}\left[\tau_\Omega^n\right] = n!\, \mathbb{E}\left[\tau_\Omega\right]$ $(n \geq 1)$ at the leading order in ϵ. The latter identity indicates that the FPT distribution of τ_Ω converges to an exponential distribution whose mean is the GMFPT defined by Eq. (29), as expected from Sec. C 1. We emphasize that the relation $\mathbb{E}\left[\tau_\Omega^n\right] = n!\, \mathbb{E}\left[\tau_\Omega\right]$ $(n \geq 1)$, implies that the GMFPT characterizes the whole distribution of the exit time, in contrast to the statement of Eq. (18) from Ref. [19].

Appendix D: Computational aspects

We summarize the numerical methods used to compute the FPT distribution.

(i) The Monte Carlo simulations rely on a sample of $2 \cdot 10^6$ of random walks. This sample is obtained through 2 hours of computation on 200 CPUs (3.20 GHz Intel Core$^{\text{TM}}$ i7). The home-built C++ program uses an adaptive time step method so that the time steps are given by a decreasing function with the distance to the exit.

(ii) A finite element method realized in COMSOL Multiphysics v4.2 [34] allowed to greatly reduce the computational time. For instance, the FPT probability density shown in Fig.2(a),(b) required 5 to 10 minutes on a single CPU (2, 66 GHz Intel Core $^{\text{TM}}$ i5).

(iii) The exact and approximate analytical solutions were computed in MATLAB and using the numerical Laplace inversion package INVLAP [39]. The series were truncated at $N = 100$ terms and the computational time is of the order of a few minutes on a single CPU (2, 66 GHz Intel Core $^{\text{TM}}$ i5).

[1] S Redner. *A guide to First- Passage Processes*. Cambridge University Press, Cambridge, England, 2001.

[2] S Condamin, O Bénichou, V Tejedor, R Voituriez, and J Klafter. First-passage times in complex scale-invariant media. *Nature*, 450(7166):77–80, 2007.

[3] O Bénichou, C Chevalier, B Meyer, and R Voituriez. Facilitated Diffusion of Proteins on Chromatin. *Physical Review Letters*, 106:38102, 2011.

[4] M Sheinman, O Bénichou, Y Kafri, and R Voituriez. Classes of fast and specific search mechanisms for proteins on DNA. *Reports on progress in physics. Physical Society (Great Britain)*, 75(2):026601, 2012.

[5] A Mazzolo. Properties of diffusive random walks in bounded domains. *Europhysics Letters (EPL)*, 68(3):350–355, 2004.

[6] Jurgen Reingruber and David Holcman. Diffusion in narrow domains and application to phototransduction. *Physical Review E (Statistical, Nonlinear, and Soft Matter Physics)*, 79(3):30904, 2009.

[7] B Meyer, O Bénichou, Y Kafri, and R Voituriez. Geometry-Induced Bursting Dynamics in Gene Expression. *Biophysical Journal*, 102(9):2186–2191, 2012.

[8] A Singer, Z Schuss, and D Holcman. Narrow Escape, Part II: The Circular Disk. *Journal of Statistical Physics*, 122(3):465–489, 2006.

[9] S Pillay, M J Ward, A Peirce, and T Kolokolnikov. An Asymptotic Analysis of the Mean First Passage Time for Narrow Escape Problems: Part I: Two-Dimensional Domains. 2009.

[10] C Chevalier, O Bénichou, B Meyer, and R Voituriez. First-passage quantities of Brownian motion in a bounded domain with multiple targets: a unified approach. *Journal of Physics A: Mathematical and Theoretical*, 44:25002, 2011.

[11] Samuel A. Isaacson and Jay Newby. Uniform asymptotic approximation of diffusion to a small target. *Physical Review E*, 88(1):012820, 2013.

[12] O Bénichou, C Chevalier, J Klafter, B Meyer, and R Voituriez. Geometry-controlled kinetics. *Nat Chem*, 2(6):472–477, 2010.

[13] B Meyer, C Chevalier, R Voituriez, and O Bénichou. Universality classes of first-passage-time distribution in confined media. *Physical Review E*, 83(5):51116, 2011.

[14] Binh T. Nguyen and Denis S. Grebenkov. A Spectral Approach to Survival Probabilities in Porous Media. *Journal of Statistical Physics*, 141(3):532–554, September 2010.

[15] Ian Naismith Sneddon. *Mixed boundary value problems in potential theory*. North-Holland Pub. Co., 1966.

[16] Carey Caginalp and Xinfu Chen. for an Escape Problem. 203:329–342, 2012.

[17] A Singer, Z Schuss, and D Holcman. Narrow escape, part II: The circular disk. *Journal of Statistical Physics*, 122(3):465–489, 2006.

[18] O Benichou and R Voituriez. Narrow-Escape Time Problem: Time Needed for a Particle to Exit a Confining Domain through a Small Window. *Physical Review Letters*, 100(16):168104–168105, 2008.

[19] Thiago G. Mattos, Carlos Mejía-Monasterio, Ralf Metzler, and Gleb Oshanin. First passages in bounded domains: When is the mean first passage time meaningful? *Physical Review E*, 86(3):031143, 2012.

[20] A Singer, Z Schuss, and D Holcman. Narrow Escape, Part III: Non-Smooth Domains and Riemann Surfaces. *Journal of Statistical Physics*, 122(3):491–509, 2006.

[21] T Lagache and D Holcman. Effective Motion of a Virus Trafficking Inside a Biological Cell. *SIAM J. Appl. Math.*, 68(4), 2008.

[22] H Carslaw. *Conduction of heat in solids*. Clarendon Press, Oxford, 1959.

[23] John Crank. *The Mathematics of Diffusion*. Oxford Science Publications, 1975.

[24] M. Sbragaglia and A. Prosperetti. A note on the effective slip properties for microchannel flows with ultrahydrophobic surfaces. *Physics of Fluids*, 19(4):043603, 2007.

[25] P. Joseph, C. Cottin-Bizonne, J.-M. Benoît, C. Ybert, C. Journet, P. Tabeling, and L. Bocquet. Slippage of Water Past Superhydrophobic Carbon Nanotube Forests in Microchannels. *Physical Review Letters*, 97(15):156104, 2006.

[26] C Cottin-Bizonne, C Barentin, E Charlaix, L Bocquet, and J-L Barrat. Dynamics of simple liquids at heterogeneous surfaces: molecular-dynamics simulations and hydrodynamic description. *The European Physical Journal. E, Soft matter*, 15(4):427–38, 2004.

[27] C W Gardiner. *Handbook of Stochastic Methods for Physics, Chemistry and Natural Sciences*. Springer, 2004.

[28] Milton Abramowitz. Handbook of Mathematical Functions with Formulas, Graphs, and Mathematical Tables. *American Journal of Physics*, 56(10):958, 1988.

[29] Denis Grebenkov. Efficient Monte Carlo methods for simulating diffusion-reaction processes in complex systems. 2013.

[30] A M Berezhkovskii and A V Barzykin. Extended narrow escape problem: Boundary homogenization-based analysis. *Physical Review E*, 82(1), 2010.

[31] O Bénichou, D Grebenkov, P Levitz, C Loverdo, and R Voituriez. Optimal Reaction Time for Surface-Mediated Diffusion. *Physical Review Letters*, 105:150606, 2010.

[32] O Bénichou, D Grebenkov, P Levitz, C Loverdo, and R Voituriez. Mean First-Passage Time of Surface-Mediated Diffusion in Spherical Domains. *Journal of Statistical Physics*, 142(4):657–685, 2011.

[33] J F. Rupprecht, O Bénichou, D Grebenkov, and R Voituriez. Kinetics of Active Surface-Mediated Diffusion in Spherically Symmetric Domains. *Journal of Statistical Physics*, 147(5):891–918, 2012.

[34] PhD Roger W. Pryor. *Multiphysics Modeling Using COMSOL: A First Principles Approach*. 2009.

[35] L. P. Castro, F. O. Speck, and F. S. Teixeira. Mixed Boundary Value Problems for the Helmholtz Equation in a Quadrant. *Integral Equations and Operator Theory*, 56(1):1–44, 2005.

[36] Denis Grebenkov. Efficient Monte Carlo Methods for Simulating Diffusion-Reaction Processes in Complex Systems. In *First-Passage Phenomena and Their Applications*. World Scientific Publishing Company, 2013.

[37] Samuel Temkin. *Elements of Acoustics*. American Institute of Physics, 2001.
[38] Dean G. Duffy. *Mixed Boundary Value Problems*. Chapman & Hall, 2007.
[39] J. Valsa. Invlap package (from Matlabcentral/fileexchange), 2011.